Redox Biology 76 (2024) 103342

Contents lists available at ScienceDirect

Redox Biology

journal homepage: www.elsevier.com/locate/redox

Lipocalin-2 aggravates blood-brain barrier dysfunction after intravenous thrombolysis by promoting endothelial cell ferroptosis via regulating the HMGB1/Nrf2/HO-1 pathway

Jie Liu [a,1], Shu-Yan Pang [a,1], Sheng-Yu Zhou [a], Qian-Yan He [a], Ruo-Yu Zhao [a], Yang Qu [a], Yi Yang [a,b,**], Zhen-Ni Guo [a,b,*]

[a] Stroke Center, Department of Neurology, The First Hospital of Jilin University, Chang Chun, China
[b] Neuroscience Research Center, Department of Neurology, First Hospital of Jilin University, Chang Chun, China

ARTICLE INFO

Keywords:
Hemorrhagic transformation
Lipocalin-2
Blood-brain barrier
Ferroptosis
High mobility group box 1
Intravenous thrombolysis

ABSTRACT

Background: Disruption of the blood-brain barrier (BBB) is a major contributor to hemorrhagic transformation (HT) in patients with acute ischemic stroke (AIS) following intravenous thrombolysis (IVT). However, the clinical therapies aimed at BBB protection after IVT remain limited.

Methods: One hundred patients with AIS who underwent IVT were enrolled (42 with HT and 58 without HT 24 h after IVT). Based on the cytokine chip, the serum levels of several AIS-related proteins, including LCN2, ferritin, matrix metalloproteinase-3, vascular endothelial-derived growth factor, and X-linked inhibitor of apoptosis, were detected upon admission, and their associations with HT were analyzed. After finding that LCN2 was related to HT in patients with IVT, we clarified whether the modulation of LCN2 influenced BBB dysfunction and HT after thrombolysis and investigated the potential mechanism.

Results: In patients with AIS following IVT, logistic regression analysis showed that baseline serum LCN2 ($p = 0.023$) and ferritin ($p = 0.046$) levels were independently associated with HT. A positive correlation between serum LCN2 and ferritin levels was identified in patients with HT. In experimental studies, recombinant LCN2 (rLCN2) significantly aggravated BBB dysfunction and HT in the thromboembolic stroke rats after thrombolysis, whereas LCN2 inhibition by ZINC006440089 exerted opposite effects. Further mechanistic studies showed that, LCN2 promoted endothelial cell ferroptosis, accompanied by the induction of high mobility group box 1 (HMGB1) and the inhibition of nuclear translocation of nuclear factor E2-related factor 2 (Nrf2) and heme oxygenase-1 (HO-1) proteins. Ferroptosis inhibitor ferrostatin-1 (fer-1) significantly restricted the LCN2-mediated BBB disruption. Transfection of LCN2 and HMGB1 siRNA inhibited the endothelial cell ferroptosis, and this effects was reversed by Nrf2 siRNA.

Conclusion: LCN2 aggravated BBB disruption after thrombolysis by promoting endothelial cell ferroptosis via regulating the HMGB1/Nrf2/HO-1 pathway, this may provide a promising therapeutic target for the prevention of HT after IVT.

1. Introduction

Acute ischemic stroke (AIS) is a leading cause of disability and death worldwide [1]. Intravenous thrombolysis (IVT) is one of the most effective therapies for AIS. However, nearly half of the patients with AIS cannot benefit from IVT, and the complications after IVT, particularly hemorrhagic transformation (HT) [2,3], cannot be ignored. The mechanism of HT after IVT is complicated, and disruption of the blood-brain barrier (BBB) is considered a major cause [4–7]. However, the clinical therapies targeting the BBB after IVT are limited. Therefore, in-depth research on the mechanisms of BBB disruption after IVT and the identification of new therapeutic targets are necessary for the prevention of HT.

Nowadays, lipocalin-2 (LCN2), a secreted circulatory protein

* Corresponding author. Department of Neurology, the First Hospital of Jilin University. Xinmin Street 1#, 130021, Changchun, China.
** Corresponding author. Department of Neurology, the First Hospital of Jilin University. Xinmin Street 1#, 130021, Changchun, China.
E-mail addresses: yang_yi@jlu.edu.cn (Y. Yang), zhen1ni2@jlu.edu.cn (Z.-N. Guo).
[1] These authors have contributed equally to this work.

https://doi.org/10.1016/j.redox.2024.103342
Received 29 July 2024; Received in revised form 25 August 2024; Accepted 3 September 2024
Available online 5 September 2024

belonging to the lipocalin superfamily, has attracted increased attention in the field of brain disorders. Under normal physiological conditions, LCN2 is produced in low amounts in the central nervous system [8], but it could be rapidly upregulated in response to injury, infection, or other inflammatory stimuli to control diverse cellular processes [9–11]. Several clinical studies have demonstrated that LCN2 protein levels in the blood/cerebrospinal fluid of patients with acute stroke were significantly elevated and can be used as an independent predictor of the poor prognosis [12–14]. An important mechanism is that, increased LCN2 contributes to BBB disruption to aggravate stroke injury [15,16]. However, the potential role of LCN2 in HT following IVT and the possible mechanisms have not been reported yet. In addition, ferritin [17,18], matrix metalloproteinase-3 (MMP-3) [19], vascular endothelial-derived growth factor (VEGF) [20], and X-linked inhibitor of apoptosis (XIAP) [21] are considered to be associated with the prognosis of AIS (Table 1). And their effects on HT following IVT remain unclear and need to be investigated further. Therefore, in this study, we sought to (1) measure the serum levels of LCN2, ferritin, MMP-3, VEGF and XIAP proteins in 100 patients with AIS after IVT and analyze their associations with HT; and (2) investigate whether the modulation of differentially expressed proteins could influence BBB function and HT after IVT in experimental stroke models as well as the potential mechanisms. Based on these, this study may pave the way for the development of novel therapeutic targets to prevent HT after IVT.

2. Methods

2.1. Participants and the study protocol

Written informed consent was obtained from all the participants. This prospective observational study followed the "Strengthening the Reporting of Observational Studies in Epidemiology (STROBE)" guidelines, and the study protocol was approved by the Ethics Committee of the First Hospital of Jilin University (2015-156). The participants had the right to withdraw from the study at any point. The animal study protocol was approved by the Ethics Committee of Jilin University, and all procedures were performed in accordance with the National Institutes of Health Guidelines on the Use of Laboratory Animals and the ARRIVE guidelines.

2.2. Clinical study

2.2.1. Study design

Patients (≥18 years of age) with AIS who received recombinant tissue plasminogen activator (rt-PA) at a dosage of 0.9 mg/kg within 4.5 h of stroke onset were enrolled from the Department of Neurology at the First Hospital of Jilin University between June 2015 and October 2017. We excluded patients who (1) underwent combined endovascular and IVT interventions; (3) had a premorbid modified Rankin Scale (mRS) score ≥2; and (4) had other neurological disorders, myocardial infarction or unstable angina within the past 6 months. To obtain reference values, we included a total of 198 patients with AIS who underwent IVT: 42 patients who presented with HT were included in the HT group, and 58 patients who received IVT but did not present with HT were enrolled in the non-HT group. Computer-based randomization was used to select 58 of 156 patients without HT.

Baseline information and clinical parameters expected to influence HT were collected, including sex, age, vascular risk factors (smoking, hypertension, diabetes, atrial fibrillation, and history of stroke), baseline National Institutes of Health Stroke Scale score (NIHSS) score, onset to thrombolysis time, baseline systolic blood pressure, systolic blood pressure, laboratory data (baseline blood glucose, platelet, and low-density lipoprotein cholesterol levels), body mass index (BMI), and international normalized ratio (INR). HT was defined as any new intracranial hemorrhage detected by computed tomography 24 h after IVT but not detected prior to IVT [22] and was classified as hemorrhagic infarction type 1 (HI1), hemorrhagic infarction type 2 (HI2), parenchymal hematoma type 1 (PH1), or parenchymal hematoma type 2 (PH2). PH was determined by dichotomizing the lesion volume to more than 30 %.

Table 1
Serum protein biomarkers and their relationship with AIS.

Biomarkers	Relationship with AIS
Ferritin	A protein that serves as body iron reservoir to store excess iron, which can induce iron overload and is an important predictor of HT after AIS [67,68].
LCN2	An acute-phase protein to regulate inflammation, which is associated with unfavorable outcomes of AIS [15,53].
MMP-3	One of the best-studied of the matrix metalloproteinases, which can lead to aberrant proteolysis and BBB dysfunction, and contribute to a worsen prognosis of AIS [69].
VEGF	A protein that participates in atherosclerosis, neuroprotection, neurogenesis, and angiogenesis. In the acute phase of AIS, its up-regulation aggravated hemorrhage risk [70–72].
XIAP	A protein that can inhibit ischemia/hypoxia-induced apoptotic cell death [73].

Abbreviations: HT, hemorrhagic transformation; AIS, acute ischemic stroke; BBB, blood-brain barrier; LCN2, lipocalin-2; MMP, matrix metalloproteinase; VEGF, vascular endothelial-derived growth factor; XIAP, X-linked inhibitor of apoptosis.

2.2.2. Serum protein measurements

Blood samples were collected from each participant on admission for serum protein detection. Samples were centrifuged at 4 °C, and the supernatant was frozen at −80 °C until use. Serum proteins were detected by the Quantibody Human custom array (RayBiotech, Norcross, GA, USA) [23]. Measurements were performed according to the manufacturer's instructions, and the signal values were analyzed using the RayBiotech analysis tool. Each sample was analyzed in four technical replicates. The clinical investigators were blinded to the serum test results until the end of the study period.

2.3. Preclinical study

2.3.1. Animals

Male Sprague-Dawley rats (weighing 250–300 g) obtained from Vital River Laboratory Animal Technology Co., Ltd. (Beijing, China) were used in the study according to an established protocol. The rats were housed in a specific pathogen-free (SPF) environment at 22–24 °C under standard 12-h light/12-h dark conditions, with free access to food and water.

2.3.2. Study design

Two animal models were established in rats, including the photothrombotic stroke (PTS) model specifically for BBB permeability evaluation and the thromboembolic stroke model in combination with rt-PA treatment for the simulation of IVT therapy after AIS in clinical settings.

In the first experiment, 34 rats were randomly assigned to undergo PTS operation or the sham operation. Rats in the PTS group were administered an intraventricular injection of recombinant LCN2 (rLCN2, 0.2, 0.4, or 0.8 μg/kg) before the surgery, and rats in the sham group were administered only phosphate-buffered saline (PBS). The dosages of rLCN2 were selected according to the previous study [24]. At 2 h before the surgery, IR-808 dyes (5 μM, 2 ml/g) were injected into the tail veins of rats. Based on NIR-II fluorescence imaging, the vascular network and leakage of fluorescent dyes in the rat brains were clearly observed. Rats were sacrificed after the last observaion. Finally, 29 rats were included, and 5 rats were excluded due to death within 72 h after surgery.

In the second experiment, 360 rats were randomly assigned to undergo the sham operation or the thromboembolic stroke surgery combined with rt-PA treatment. Rats in each group were administered an intraventricular injection of rLCN2 (the dosage depended on the results

of the first part) or an equal volume of PBS 1 h before the surgery or were intraperitoneally injected with ZINC00640089 (25 mg/kg, the inhibitor of LCN2) or an equal volume of 10 % DMSO 1 h before the surgery and 8 h after thrombolysis, respectively. To clarify the potential role of ferroptosis in LCN2-enhanced BBB disruption after thrombolysis, the thromboembolic stroke rats were intraperitoneally injected with ferrostatin-1 (fer-1) (10 mg/kg) or an equal volume of 5 % DMSO 2 h before the surgery. At different time points after thrombolysis, rats were sacrificed for further analysis. Finally, 347 rats were included, and 13 rats were excluded due to the lack of neurological deficit 1 h after surgery or dying before the analysis points. All behavioral measures and data analyses were performed in a blinded manner.

In the in vitro studies, oxygen and glucose deprivation/reoxygenation (OGD/R) (6h/12h) and rt-PA stimulation (100 μg/mL) at the start of reoxygenation were introduced into Bend.3 endothelial cells based on our preliminary tests to mimic BBB damage after thrombolysis. In different experiments, rLCN2 (200 ng/ml) was administered 2 h before OGD/R; fer-1 (5 μM, dissolved in 0.1 % DMSO) was administered 4 h before OGD/R; and transfection of different small interfering ribonucleic acid (siRNA) was performed 24 h before OGD/R. After reoxygenation for 12 h, the cells and supernatants were collected for further analysis. The detailed experimental designs and source of reagents are listed in Supplemental Method.

2.3.3. Animal surgery

Two animal models were used in this study. The thromboembolic stroke model was established as previously described, with minor modifications [25,26]. Briefly, rats were anesthetized with 4 % isoflurane in an air/oxygen (70/30) mixture and maintained with 1.5 % isoflurane through a facemask during the surgery period. The right common carotid artery (CCA) was exposed and isolated via midline incision, and its branches were also dissected and coagulated. Then, the CCA was placed in the electric clamp of the YLS-148 thrombus formation tester (Jinan Yiyan Science & Technology Development Co., Ltd.), and the distal CCA was clamped using an artery clamp. Galvanic stimulation (1.00 mA) was initiated for 90 s to induce the formation of thrombus. After that, the thrombus was fragmented into pieces with microscopic tweezers until the blood vessels exhibited a uniform gray color and resumed pulsation, indicating restoration of blood flow. The CCA was temporarily released to direct the crushed thrombus towards the middle cerebral artery/lacunar artery and the internal carotid artery. Later, the CCA was re-clamped and stimulated (1.00 mA) for another 240 s to form an additional thrombus. After that, the artery clamp was relieved, and the crushed thrombus was flushed into the internal carotid artery. Finally, the CCA was clamped for another 10 min to stabilize the thrombus. Three hours after ischemia, the rats were anesthetized again and administered 10 mg/kg rt-PA via the tail vein. The initial 10 % dose of rt-PA was administered within 1 min, whereas the remaining 90 % was infused over 10 min using a syringe infusion pump (RWD Life Science Co., Ltd., Shenzhen, China). Rats in the sham group underwent the same procedure without galvanic stimulation and were injected intravenously with an equal volume of saline through the tail vein 3 h after embolus insertion.

The PTS model was established as previously described. At first, rats were injected with Rose Bengal (4,5,6,7-tetrachloro-2′,4′,5′,7′-tetraiodofluorescein, RB, 50 mg/ml) through the tail vein. The thinned skull was then irradiated with a circular 561 nm laser for 15 min to induce thrombus formation. Rats injected with PBS before irradiation were used as sham-operated controls.

2.3.4. Intracerebral ventricular injections

Intracerebral ventricular injections were administered as previously described [27]. Briefly, the rats were positioned in a stereotactic apparatus, and a cranial burr hole (1 mm) was drilled. A total volume of approximately 10 μl rLCN2 or PBS was injected into the ipsilateral ventricle of rats using a 10-μl Hamilton syringe at a rate of 0.5 μL/min via a microinjection pump before the surgery (coordinates: 0.5 mm posterior, 1.6 mm lateral, and 4.8 mm ventral to the bregma).

2.3.5. Assessment of neurological deficits

At 24 h after thrombolysis, we assessed the neurological deficits of rats. The Zea Longa score [28], modified Garcia score [29], the forelimb placing test [30], corner turn [31] test, and horizontal ladder walking task [32] were performed and scored in a blinded fashion, as previously described.

The Zea Longa score: The performance of rats were scored as follows: 0 points, no observable neurologic deficit; 1 point, failed to extend the right forepaw; 2 points, circled to the right; 3 points, unable to walk spontaneously; and 4 points, dead.

Modified Garcia score: The score comprises six tested items: spontaneous activity, reaction to touch on both sides of the trunk, spontaneous movement of all limbs, movement of the forelimbs, response to vibrissa touch, and climbing. The total score ranges from 3 (most severe deficit) to 18 (no deficit).

Forelimb placement test: Rats were held by their torsos, which allowed the forelimb to hang free, and were then placed on the corner edge of the table to stimulate the vibrissae. When the rat's vibrissae touched the table, the ipsilateral foreleg movement on the table responded to the vibrissae stimulation. Ten trials were performed for each rat, and the percentage of successful responses was calculated.

Corner turn test: Rats were allowed to approach a corner at an angle of 30°. When the rat tried to exit the corner, its choice of either a left or right turn was recorded. This trial was repeated ten times for each rat. The percentage of left turns was then calculated.

Horizontal ladder walking task: The apparatus consisted of sidewalls made of clear Plexiglas and stainless-steel rungs (3 mm diameter). The sidewalls were 1 m long and 20 cm high and equipped with 99 evenly spaced holes at the bottom, each spaced 1 cm apart, for the insertion of stainless-steel rungs. Rungs were randomly inserted into the holes (spacing between bars ranged from 1 to 3 cm). The ladder was set 30 cm above the ground. The rats walked spontaneously from the beginning to the end of the horizontal ladder, and a camera was placed on the lateral ventral side to record paw activity. The trial was repeated ten times for each rat, and the total number of limb drops were calculated.

2.3.6. Infarct measurement

At 24 h after thrombolysis, rats were euthanized, and their brains were removed and sliced coronally into 2-mm-thick sections. These sections were then stained with 1 % 2,3,5-triphenyltetrazoliumchloride (TTC, Sigma, USA) solution at 37 °C for 20 min in the dark. The infarct volume was calculated with edema correction using ImageJ software (Wayne Rasband, National Institutes of Health, USA) [33].

2.3.7. Intracerebral hemorrhage detection

Rats were transcardially perfused with PBS to remove intravascular blood 24 h after thrombolysis. The brains were separated into ipsilateral and contralateral hemispheres. For quantitative measurement, the ipsilateral hemisphere was homogenized with 300 μl PBS in a FastPrep-24 5 G homogenate device (MP Biomedicals) for 1 min and centrifuged at 13,000×*g* for 30 min. Next, Drabkin reagent was added to the supernatant and incubated for 15 min. The absorbance was measured at 540 nm with a spectrophotometer (Spectronix 3000, Milton-Roy, Rochester, NY) and hemorrhage volume (μL) was calculated using a standard curve.

2.3.8. BBB permeability evaluation

Two methods were used to evaluate the BBB permeability of rats.

IR-808 dyes (5 μM, 2 ml/g) were introduced into PTS rats via tail vein injections 2 h before the surgery. Based on NIR-II fluorescence imaging, the vascular network and leakage of fluorescent dyes in the brain of rats were clearly observed. Gray values difference between the ipsilateral and contralateral hemispheres were calculated at different

time points to assess variations in BBB permeability. The gray value difference before the surgery was set to 0 in each rat.

Rats that underwent thromboembolic stroke surgery and received rt-PA treatment were anesthetized and injected with Evans Blue (EB) 24 h after thrombolysis (2 mL/kg, 4 % in saline). After 4 h of circulation, rats were transcardially perfused with PBS to remove intravascular blood and the ipsilateral brain hemispheres were collected and homogenized with a 50 % trichloroacetic acid solution in a FastPrep-24 5 G homogenate device for 1 min. The mixture was then centrifuged at 13,000g, 4 °C for 15 min. The absorbance of the supernatant at 620 nm was measured using a spectrophotometer to quantify the extravasation of EB dye and then compared with a standard curve.

2.3.9. Cell culture and OGD/R model

The Bend.3 mouse brain endothelial cell line was obtained from FuHeng Cell Center (Shanghai, China) and cultured in Dulbecco's modified Eagle's medium (DMEM; Gibco, Carlsbad, CA, USA) supplemented with 10 % fetal bovine serum (FBS; Invitrogen, Carlsbad, CA, USA) and 1 % penicillin-streptomycin (Sigma-Aldrich, St. Louis, MO, USA) in a humidified incubator at 37 °C, with 5 % CO2. To induce OGD/R injury, we transferred cells to glucose- and FBS-free DMEM and incubated them in a hypoxic chamber filled with 5 % CO2/95 % N2 at 37 °C for 6 h. Then, the medium was discarded, and the cells were returned to normal culture conditions for re-oxygenation [34].

2.3.10. Cell counting kit-8 (CCK8) assay

CCK8 was used to determine cell viability according to the manufacturer's protocol [35]. Briefly, Bend.3 cells were seeded in 96-well plates. After reoxygenation, the conditioned medium was refreshed, and 10 μl of CCK8 reagent (Solarbio, Japan) was added to each well, followed by further incubation for 2 h. The absorbance was measured at 450 nm using a spectrophotometer.

2.3.11. Transfection of siRNA

Bend.3 cells were seeded in 6-well plates before siRNA transfection. The sequence of high mobility group box 1 (HMGB1) siRNA was sense 5′-GCAGCCCUAUGAGAAGAAATT-3,' antisense 5′-UUUCUUCUCAUAGGGCUGCTT-3'; the LCN2 siRNA sequence was sense 5′-GCCUCAAGGACGACAACAUTT-3,' antisense 5' -AUGUUGUCGUCCUUGAGGCTT-3'; the Nrf2 siRNA sequence was sense 5′-GCCUCAAGGACGACAACAUTT-3,' antisense 5' -AUGUUGUCGUCCUUGAGGCTT-3'; the 24p3r siRNA sequence was sense 5′-GCCUCAAGGACGACAACAUTT-3,' antisense 5' -AUGUUGUCGUCCUUGAGGCTT-3'. Transfection was performed using HiPerfect transfection reagent (Qiagen, Germany) according to the manufacturer's protocol. To evaluate transfection efficiency, we harvested cells and supernatants and subjected them to Western Blot (WB) and enzyme linked immunosorbent assay (ELISA).

2.3.12. Measurement of Glutathione (GSH), malondialdehyde (MDA), iron content and ROS

GSH, MDA, and cell iron content were measured from protein lysates of rat brains or Bend.3 cells following the manufacturer's instructions. The concentration of GSH was expressed as μg/g sample (in vivo study), or μg/10^6 cells (in vitro study); the concentration of MDA was expressed as μmol/g sample (in vivo study) or μmol/10^6 cells (in vitro study). Iron concentrations were expressed as ng/10^6 cells (in vitro study).

Intracellular ROS levels were measured using 2′,7′-Dichlorofluorescin diacetate (DCFH-DA). Briefly, the collected cells were incubated with 10 μM DCFH-DA (dissolved in serum-free medium) at 37 °C for 20 min in the dark. After washing with serum-free medium three times, the fluorescence intensity was detected using a flow cytometer (Becton, Dickinson and Company, New Jersey, USA) and analyzed using FlowJo analytical software (TreeStar).

2.3.13. Immunofluorescence (IF) staining

Rats were sacrificed after perfusion, and their brains were fixed using 4 % PFA and dehydrated with sucrose gradient. Then, the brains were embedded in an Optimal Cutting Temperature compound for frozen sections and sliced into 10-μm sections. After washing with PBS for 20 min, the slices were blocked with 10 % goat serum for 1 h. Following this, they were incubated with primary antibodies at 4 °C overnight, and then incubated with species-specific Alexa Fluor-488/594-conjugated secondary antibodies for 1 h in the dark. Fluoroshield™ with DAPI was used for nuclear staining. Images were captured using a FluoView FV3000 confocal laser scanning microscope (Olympus, Tokyo, Japan) with × 20 and × 60 objectives. The percentage of positive cells was calculated using ImageJ software. Three rats were used per experimental group, with at least three regions selected for analysis in each rat [36].

2.3.14. WB

Protein samples from the rat brains and cultured cells were extracted using RIPA-lysis buffer. Cytoplasmic and nuclear proteins were extracted using the Nuclear and Cytoplasmic Protein Extraction Kit (Beyotime), according to the manufacturer's protocols. Proteins was separated on a 4–12 % polyacrylamide gel and transferred onto polyvinylidene difluoride membranes. The membranes were then blocked with 5 % skim milk at room temperature for 1 h and incubated at 4 °C overnight with primary antibodies. Subsequently, the membranes were incubated with the corresponding HRP-conjugated secondary antibodies at room temperature for 1 h. Protein bands were detected with an ECL kit and quantified using ImageJ software. For sequential blotting, the membranes were stripped with a Stripping Buffer and reprobed with the appropriate antibodies. LaminB 1 served as a loading control for nuclear fractions, and β-actin served as a loading control for cytoplasmic fractions and total proteins to normalize protein levels [37].

2.3.15. ELISA

The levels of LCN2 and HMGB1 in the brain lysate and serum of rats or supernatant of Bend.3 cells were examined using ELISA kits. Measurements were performed according to the manufacturer's instructions. The absorbance was measured at 450 nm, and the concentration was calculated using standard curve interpolation. Each experiment was performed in triplicate.

2.3.16. Statistical analyses

All data were analyzed using SPSS 26.0 version (SPSS Inc., Armonk, NY, USA) and GraphPad Prism version 8.0 (GraphPad Software, San Diego, CA, USA). Continuous data were described as the mean ± standard deviation (SD) or median and interquartile ranges according to distribution. Two-group comparisons were conducted using Student's t-test or the Mann-Whitney *U* test. Multiple group comparisons were analyzed using one-way ANOVA, two-way ANOVA or the Kruskal-Wallis H test with Tukey's correction (in the preclinical study). Univariate and multivariate logistic regression analyses were performed to investigate the association between serum protein levels and HT after IVT in patients with AIS. Count data were expressed as absolute values and percentages and were analyzed using the $\chi 2$ test or Fisher exact test. Serum protein levels were converted into binary variables based on the median values. A p-value of <0.05 was considered statistically significant.

3. Results

3.1. Association between serum proteins and HT

This study included 100 patients with AIS who underwent IVT, comprising 42 patients with HT and 58 patients without HT. Among the patients with HT, 23 had HI (HI1 in 8, HI2 in 15), and 19 had PH (PH1 in 11, PH2 in 8). The demographic and baseline characteristics of the included patients were compared across the HT in Supplemental

Table 1.

Based on the cytokine chip, we measured the serum levels of five AIS-associated proteins in these patients on admission, including LCN2, ferritin, MMP-3, VEGF, and XIAP. The comparison of serum protein levels among different groups is shown in Table 2. We found that MMP-3 ($p = 0.012$) and VEGF ($p = 0.047$) levels were significantly lower in the HT group than in the non-HT group. After adjusting for possible confounding factors, the multivariate logistic analysis revealed that higher levels of ferritin (OR 1.589; 95 % CI 1.008–2.505; $p = 0.046$) and LCN2 (OR 3.17; 95 % CI 1.271–8.581; $p = 0.023$) were independently associated with the increased risk of HT (Table 3).

Subsequently, we investigated the relationship between the serum level of LCN2 and other proteins. Interestingly, Spearman correlation analysis revealed a significant positive correlation between serum LCN2 and ferritin levels in patients with HT (rs = 0.675, $p < 0.001$). The correlation coefficient was higher in patients with PH (rs = 0.789, $p < 0.001$) than in those with HI (rs = 0.676, $p < 0.001$) (Fig. 1). As previously reported, ferritin is considered to be critically associated with the induction of iron overload and overproduction of reactive oxygen species after AIS, which are characteristic processes that lead to ferroptosis [38,39]. Therefore, we speculated that LCN2 may be positively correlated with ferroptosis in IVT-induced HT.

3.2. rLCN2 promoted BBB disruption and HT after thrombolysis

Animal studies were conducted to critically assess the role of LCN2 in BBB disruption and HT after thrombolysis. First, we established a PTS model in rats. IR-808 dyes (5 μM, 2 ml/g) were injected into the tail vein of rats 2 h before the surgery, and the accumulation of the fluorescent dye was detected based on the NIR-II imaging. rLCN2 protein was introduced via intraventricular injection before the surgery to mimic the secretion of LCN2 during AIS. We observed that rLCN2 significantly aggravated BBB permeability in the ipsilateral hemisphere of rats in the PTS group during a 72-h course, especially within 24 h after surgery, and that rLCN2 at 0.8 μg/kg exerted similar effects compared with rLCN2 at 0.4 μg/kg (Fig. 2). Therefore, in following experiments, we primarily investigated the effects of LCN2 at 24 h after AIS and chosen 0.4 μg/kg as the appropriate dose of rLCN2.

Then, a thromboembolic stroke rat model combined with rt-PA thrombolysis was established to simulate clinical IVT therapy after AIS. According to WB and ELISA analysis, we observed a remarkable elevation of LCN2 levels in the brain of rats at 3 h after surgery (before thrombolysis) and a gradual increase over the following 24 h after thrombolysis. rLCN2 treatment further promoted this trend (Fig. 3A). This phenomenon was consistent with ELISA findings that reflect serum LCN2 levels, indicating the successful transmission of rLCN2 between brain and serum (Fig. 3A). Based on this, the neurological deficits, cerebral infarction, hemorrhage volumes, and BBB function of rats were tested 24 h after thrombolysis. Compared with the sham operation, the thromboembolic stroke surgery followed by rt-PA thrombolysis induced obvious neurobehavioral defects (Fig. 3B), cerebral infarction (Fig. 3C), hemorrhage (Fig. 3D), Evans blue (EB) dye extravasation (Fig. 3E) and the downregulation of tight junction proteins (TJPs), including ZO-1, occludin, and claudin-5 (Fig. 3F). And rLCN2 supplementation further aggravated cerebral damage in stroke rats and promoted BBB disruption (Fig. 3C–F).

Table 2
Comparison of baseline serum protein levels between patients in different groups.

Indicators (pg/ml)	HT group (n = 42)	Non-HT group (n = 58)	Z	*p*
Ferritin	29458.29 (23860.56, 32962.88)	24455.33 (19559.58, 32271.69)	−1.488	0.137
LCN2	6542.04 (6175.42, 7101.10)	6368.16 (5611.47, 7082.52)	−1.592	0.111
MMP-3	57223.33 (33254.64, 95628.82)	77985.79 (51095.32, 119596.44)	−2.514	**0.012**
VEGF	440.87 (240.59, 619.81)	575.71 (311.04, 998.58)	−1.983	**0.047**
XIAP	0 (0, 4.21)	0 (0, 11.66)	−1.1	0.271

Abbreviations: HT, hemorrhagic transformation; LCN2, lipocalin-2; MMP, matrix metalloproteinase; VEGF, vascular endothelial-derived growth factor; XIAP, X-linked inhibitor of apoptosis.

Table 3
Association between serum protein levels and HT.

Variables	Model 1		Model 2		Model 3	
	OR (95 % CI)	*p*	OR (95 % CI)	*p*	OR (95 % CI)	*p*
Ferritin	1.39 (0.93, 2.09)	0.107	1.502 (0.987, 2.285)	0.058	1.589 (1.008, 2.505)	**0.046**
LCN2	1.641 (0.737, 3.655)	0.225	1.957 (0.844, 4.534)	0.118	3.17 (1.271, 8.581)	**0.023**
MMP-3	0.434 (0.193, 0.979)	0.044	0.477 (0.203, 1.123)	0.09	0.5 (0.198, 1.268)	0.144
VEGF	0.515 (0.23, 1.153)	0.107	0.491 (0.207, 1.164)	0.106	0.4 (0.155, 1.032)	0.058
XIAP	0.85 (0.38, 1.88)	0.685	0.753 (0.328, 1.727)	0.503	0.667 (0.271, 1.637)	0.376

Model 1: Unadjusted.
Model 2: Adjusted for sex, age, baseline NIHSS.
Model 3: Adjusted for sex, age, baseline NIHSS, and variables with $p < 0.15$ (including smoking, history of stroke, onset to thrombolysis time, and baseline blood glucose).
Abbreviations: HT, hemorrhagic transformation; OR, odds ratio; CI, confidence interval; NIHSS, National Institute of Health stroke scale; LCN2, lipocalin-2; MMP, matrix metalloproteinase; VEGF, vascular endothelial-derived growth factor; XIAP, X-linked inhibitor of apoptosis.

3.3. Pharmacological inhibition of LCN2 alleviated BBB disruption and HT after thrombolysis

ZINC00640089 is a newly discovered specific inhibitor of LCN2 [40]. To further clarify the effects of LCN2 on BBB disruption and HT after thrombolysis, we introduced ZINC00640089 into rats. According to our preliminary results, intraperitoneal injection of ZINC00640089 (25 mg/kg) 1 h before the surgery and 8 h after thrombolysis significantly decreased the expressions of LCN2 protein both in serum and brain of rats (Fig. 4A). Meanwhile, it also tended to alleviate neurobehavioral deficits (Fig. 4B), and significantly reduced cerebral infarction (Fig. 4C), hemorrhage (Fig. 4D), EB dye extravasation (Fig. 4E) and the downregulation of TJPs compared to the vehicle group (Fig. 4F), suggesting notable protective effects by LCN2 inhibition.

3.4. LCN2 promoted BBB disruption after thrombolysis by inducing endothelial cell ferroptosis

Since the contribution of LCN2 to BBB disruption after thrombolysis has been demonstrated, we then focused on its potential mechanism. The cellular locations of LCN2 and its specific receptor 24p3r [41] in ischemic cortex were clarified with co-IF staining. The results showed that LCN2 was significantly upregulated and substantially co-localized with astrocyte marker (GFAP) and endothelial cell marker (CD31) 24 h after thrombolysis (Fig. 5A), whereas its receptor 24p3r could be co-localized with neuronal marker (NeuN), microglial marker (IBA1), GFAP, and CD31 (Fig. 5B), which indicated that LCN2 was mainly released by astrocytes and endothelial cells and could act on neurons,

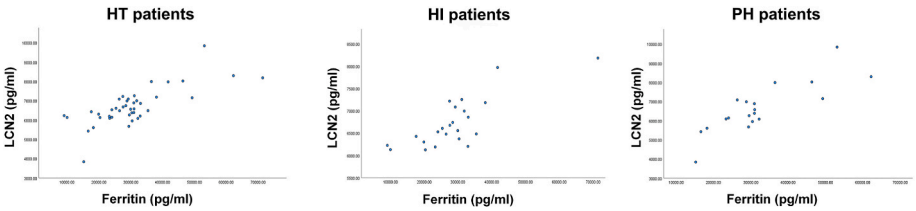

Fig. 1. The correlation between the serum levels of LCN2 and ferritin in patients with HT.

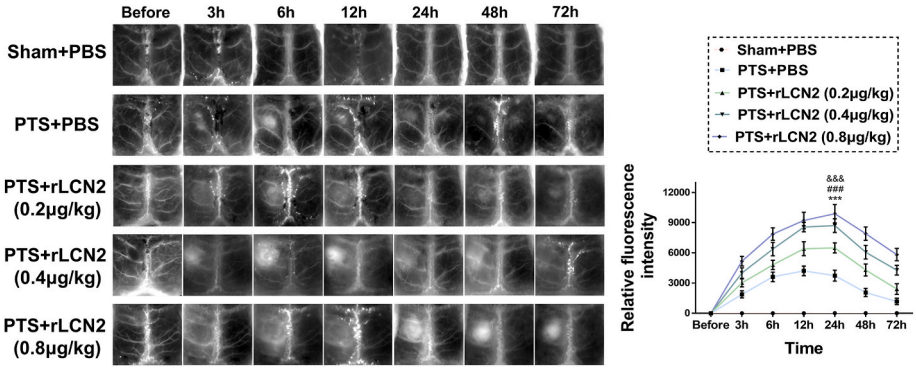

Fig. 2. Increased LCN2 aggravated BBB disruption in PTS rats. Representative photographs of NIR-II imaging of rats and quantitative analyses of the fluorescent dye accumulation (μg/g tissue) before and at 3 h, 6 h, 12 h, 24 h, 48 h, and 72 h after surgery. n = 5–6/group. ***$p < 0.001$ PTS + rLCN2 (0.2 μg/kg) vs PTS + PBS; ###$p < 0.001$ PTS + rLCN2 (0.4 μg/kg) vs PTS + PBS; &&&$p < 0.001$ PTS + rLCN2 (0.8 μg/kg) vs PTS + PBS by two-way ANOVA ($F = 543.35$, $p < 0.001$ for different time points and $F = 1221.36$, $p < 0.001$ for different dosage of drugs).

microglia, astrocytes, and endothelial cells after thrombolysis.

Based on our clinical speculation, LCN2 may be positively associated with ferroptosis in IVT-induced HT. In addition, ferroptosis of cerebrovascular endothelial cells, a critical component of the BBB, has been repeatedly identified to promote BBB dysfunction in cerebrovascular diseases [42–44]. Therefore, we examined whether LCN2 contributes to BBB disruption after thrombolysis by modulating the ferroptosis of endothelial cells. Ferroptosis damage was assessed by detecting the expressions of PTGS2, FTH1, and GPX4 proteins and measuring GSH and MDA levels. The results showed that the expressions of PTGS2 and MDA were markedly elevated, whereas the expressions of FTH1, GPX4, and GSH were decreased in the brain of thromboembolic stroke rats compared with the sham rats 24 h after thrombolysis (Fig. 5C-D). Meanwhile, a high percentage of PTGS2-positive endothelial cells was also identified in the ischemic cortex of the thromboembolic stroke rats. rLCN2 administration further enhanced these changes, whereas ZINC00640089 reversed these damages (Fig. 5E).

Then, to clarify the crosstalk between the LCN2-mediated ferroptosis and BBB disruption after thrombolysis, we used the ferroptosis inhibitor, fer-1. As illustrated in Fig. 5F, fer-1, similar to ZINC00640089, alleviated the decrease of TJPs in thromboembolic stroke rats. Meanwhile, additional administration of fer-1 also reversed the downregulation of TJPs induced by rLCN2. Therefore, we proposed that LCN2 could induce BBB dysfunction after thrombolysis by promoting endothelial cell ferroptosis and that targeting LCN2 inhibition might be a promising therapeutic approach to prevent HT.

To further seek in vitro evidence confirming these results, we conducted studies using Bend.3 endothelial cells. A combination of OGD/R and rt-PA stimuli was used to simulate IVT-induced BBB damage after AIS. CCK8 assay showed that cell viability was significantly decreased after different OGD/R conditions and that 6-h OGD decreased cell viability by about 45 % (Fig. 6A); In addition, LCN2 levels were upregulated and reached the highest levels at 12 h of reoxygenation after 6-h OGD (Fig. 6B). Thus, we selected OGD/R (6h/12h) as the optimal time points for experiments. rLCN2 and LCN2 siRNA were used to modulate the expression of LCN2 in Bend.3 cells and fer-1 was used to inhibit ferroptosis. The successful transfection of siRNA was confirmed with WB and ELISA (Supplemental Fig. 1). In agreement with the in vivo findings, our results showed that after exposure to OGD/R + rt-PA stimulus, the levels of PTGS2, cell iron, MDA, and ROS were significantly increased, whereas the levels of TJPs, FTH1, GPX4, and GSH were significantly decreased. rLCN2 administration further enhanced these changes; however, transfection with LCN2 siRNA alleviated the damages (Fig. 6C–E). Fer-1, similar to LCN2 siRNA, mitigated OGD/R + rt-PA-induced TJPs reductions, meanwhile, it also reversed the downregulation of TJPs induced by rLCN2 (Fig. 6F).

3.5. *LCN2 induced endothelial cell ferroptosis after thrombolysis via promoting HMGB1 secretion*

HMGB1 is a classical regulatory protein of cellular ferroptosis, which is also critically involved in the pathogenesis of BBB disruption and HT after AIS [45,46]. In recent years, studies have shown that increased LCN2 could induce HMGB1 secretion by binding to its cell surface receptor 24p3r [24]. However, the potential link between LCN2 and HMGB1 in IVT-induced HT remains unclear. To further elucidate the potential signaling responsible for the endothelial cell ferroptosis mediated by LCN2 after thrombolysis, we then focused on the variation of HMGB1. In animal studies, our results showed that HMGB1 was highly increased in the brains of thromboembolic stroke rats 24 h after thrombolysis compared to sham rats (Fig. 7A), and co-IF staining also indicated a significant increase in the co-localization of HMGB1 and CD31 in the ischemic cortex, similar to LCN2. Administration of rLCN2 further upregulated HMGB1 levels and increased the percentage of HMGB1-positive endothelial cells, whereas ZINC00640089 inhibited HMGB1 expressions and decreased the percentage of HMGB1-positive endothelial cells (Fig. 7B). Consistently, in in vitro studies, we found that with OGD/R + rt-PA stimulus, rLCN2 supplementation markedly elevated the level of HMGB1 in Bend.3 cells, whereas exposure to LCN2 siRNA reversed the increase of HMGB1 (Fig. 7C). Furthermore, we found that transfection of 24p3r siRNA abolished the influence of rLCN2 on HMGB1 secretion, which suggested that LCN2 modulated HMGB1

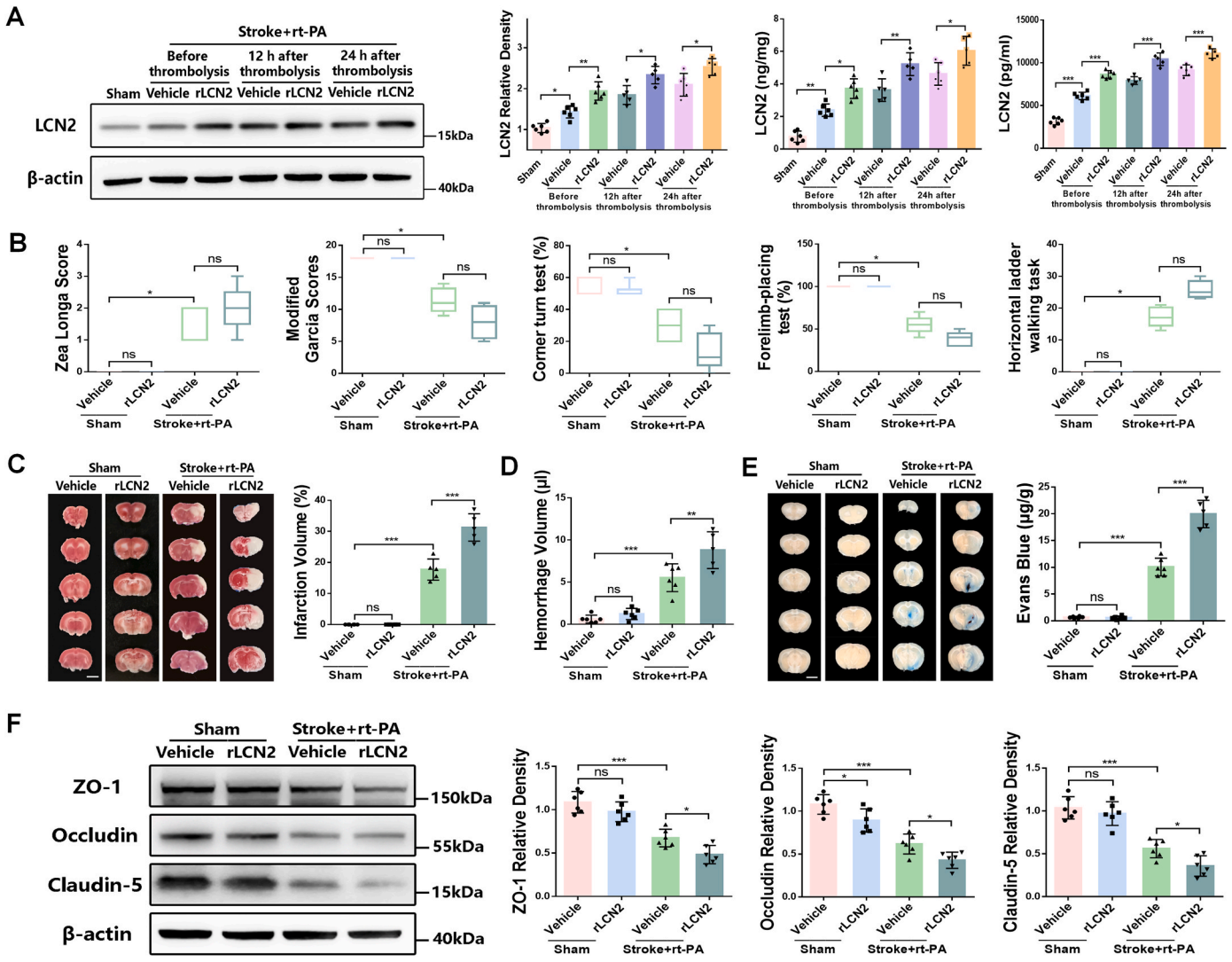

Fig. 3. Increased LCN2 aggravated cerebral damages and BBB disruption in the thromboembolic stroke rats after thrombolysis. (A) Expressions of LCN2 in the brain and serum of rats at different time points after surgery according to WB and ELISA analysis. n = 5–6/group. $^{*}p < 0.05$, $^{**}p < 0.01$, $^{***}p < 0.001$ by one-way ANOVA ($F = 34.52$, $p < 0.001$ for WB analysis of brain tissue; $F = 45.22$, $p < 0.001$ for ELISA analysis of brain tissue, and $F = 148.78$, $p < 0.001$ for ELISA analysis of serum respectively); (B) Neurological deficits of rats 24 h after thrombolysis. n = 5–6/group. $^{*}p < 0.05$ by Kruskal-Wallis H test ($H = 20.28$, $p < 0.001$ for measurement of Zea Longa score; $H = 20.3$, $p < 0.001$ for measurement of modified Garcia score; $H = 18.77$, $p < 0.001$ for measurement of corner turn test; $H = 20.67$, $p < 0.001$ for measurement of forelimb placing test and $H = 21.3$, $p < 0.001$ for measurement of horizontal ladder walking task respectively); (C) Representative coronal sections of TTC staining and quantitative analyses of cerebral infarct volume 24 h after thrombolysis. n = 5–6/group. Scale bar: 5 mm $^{***}p < 0.001$ by one-way ANOVA ($F = 179.21$, $p < 0.001$); (D) Quantification of hematoma volume (μl) 24 h after thrombolysis. n = 5–6/group. $^{**}p < 0.01$, $^{***}p < 0.001$ by one-way ANOVA ($F = 43$, $p < 0.001$); (E) Representative coronal sections of EB staining and quantitative analyses of EB dye extravasation (μg/g tissue) 24 h after thrombolysis. n = 5–6/group. Scale bar: 5 mm $^{***}p < 0.001$ by one-way ANOVA ($F = 215.84$, $p < 0.001$); (F) Expressions of ZO-1, occludin, and claudin-5 in the ipsilateral hemisphere of rats 24 h after thrombolysis. n = 6/group. $^{*}p < 0.05$, $^{***}p < 0.001$ by one-way ANOVA ($F = 36.82$, $p < 0.001$ for WB analysis of ZO-1; $F = 37.06$, $p < 0.001$ for WB analysis of occludin and $F = 41.32$, $p < 0.001$ for WB analysis of claudin-5 respectively).

expression primarily through 24p3r receptor-mediated signaling (Fig. 7D). Then, to verify whether HMGB1 was involved in LCN2-induced endothelial cell ferroptosis after thrombolysis, we introduced HMGB1 siRNA to Bend.3 cells. According to our results, HMGB1 siRNA transfection significantly reversed the increase of MDA, ROS, cell iron, and PTGS2 levels, and the decrease of FTH1, GPX4, and GSH levels induced by rLCN2 upon OGD/R + rt-PA stimulus (Fig. 7E–F). Therefore, we hypothesized that the secretion of HMGB1 induced by LCN2 contributes to endothelial cell ferroptosis after thrombolysis.

3.6. Nrf2/HO-1 signaling was involved in the LCN2/HMGB1-mediated endothelial cell ferroptosis after thrombolysis

Currently, Nrf2/HO-1 signaling is considered a classical pathway for the modulation of ferroptosis [47,48]. Some studies focusing on other diseases have showed that the inhibition of HMGB1 aggravated ferroptosis by promoting the nuclear aggregation of Nrf2 and the activation of the HO-1 protein [49,50]. Therefore, we next verified the participation of Nrf2/HO-1 pathway in LCN2/HMGB1-mediated ferroptosis of endothelial cells after thrombolysis. In animal studies, WB analysis showed that the nuclear-Nrf2 levels were highly increased in the brains of thromboembolic stroke rats 24 h after thrombolysis compared to that in the sham rats, accompanied with the upregulation of HO-1 proteins. Additional administration of rLCN2 suppressed their expressions, whereas ZINC00640089 further promoted their expressions (Fig. 8A). Consistently, in in vitro studies, LCN2 or HMGB1 siRNA transfection further facilitated the nuclear translocation of Nrf2 and the upregulation of HO-1 in Bend.3 cells upon OGD/R + rt-PA stimulus. However, rLCN2

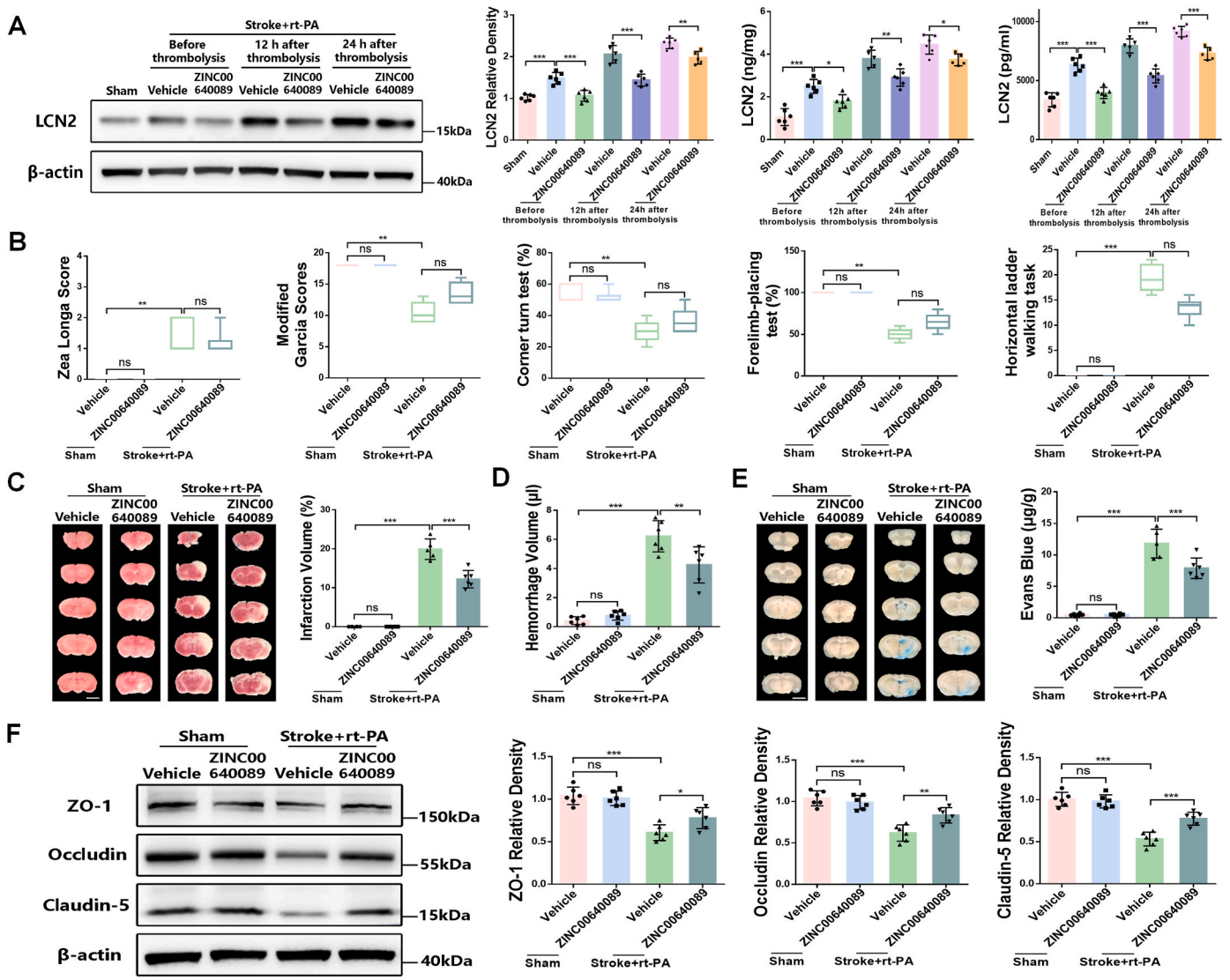

Fig. 4. Inhibition of LCN2 alleviated cerebral damages and BBB disruption in the thromboembolic stroke rats after thrombolysis. (A) Expressions of LCN2 in the brain and serum of rats at different time points after surgery according to WB and ELISA analysis. n = 5–6/group. $^{*}p < 0.05$, $^{**}p < 0.01$, $^{***}p < 0.001$ by one-way ANOVA ($F = 73.29$, $p < 0.001$ for WB analysis of brain tissue; $F = 60.3$, $p < 0.001$ for ELISA analysis of brain tissue and $F = 87.07$, $p < 0.001$ for ELISA analysis of serum respectively); (B) Neurological deficits of rats 24 h after thrombolysis. n = 5–6/group. $^{**}p < 0.01$, $^{***}p < 0.001$ by Kruskal-Wallis H test ($H = 20.38$, $p < 0.001$ for measurement of Zea Longa score; $H = 20.62$, $p < 0.001$ for measurement of modified Garcia score; $H = 16.3$, $p = 0.001$ for measurement of corner turn test; $H = 20.62$, $p < 0.001$ for measurement of forelimb placing test and $H = 21.23$, $p < 0.001$ for measurement of horizontal ladder walking task respectively); (C) Representative coronal sections of TTC staining and quantitative analyses of cerebral infarct volume 24 h after thrombolysis. n = 5–6/group. Scale bar: 5 mm $^{***}p < 0.001$ by one-way ANOVA ($F = 187.87$, $p < 0.001$); (D) Quantification of hematoma volume (μl) 24 h after thrombolysis. n = 6/group. $^{**}p < 0.01$, $^{***}p < 0.001$ by one-way ANOVA ($F = 65.51$, $p < 0.001$); (E) Representative coronal sections of EB staining and quantitative analyses of EB dye extravasation (μg/g tissue) 24 h after thrombolysis. n = 5–6/group. Scale bar: 5 mm $^{***}p < 0.001$ by one-way ANOVA ($F = 96.39$, $p < 0.001$); (F) Expressions of ZO-1, occludin and claudin-5 in the ipsilateral hemisphere of rats 24 h after thrombolysis. n = 6/group. $^{*}p < 0.05$, $^{**}p < 0.01$, $^{***}p < 0.001$ by one-way ANOVA ($F = 24.37$, $p < 0.001$ for WB analysis of ZO-1; $F = 25.49$, $p < 0.001$ for WB analysis of occludin and $F = 45.16$, $p < 0.001$ for WB analysis of claudin-5 respectively).

administration inhibited their expressions, whereas co-transfection with HMGB1 siRNA reversed these inhibitions (Fig. 8B). Further knocking down of Nrf2 showed that the expression of HO-1 was significantly inhibited, accompanied by the aggravated ferroptosis damages. And co-transfection with Nrf2 siRNA also abolished the inhibition of ferroptosis induced by LCN2 siRNA and HMGB1 siRNA (Fig. 8C–D). Hence, we proposed that LCN2 induced the secretion of HMGB1 and inhibition of Nrf2/HO-1 pathway to promote endothelial cell ferroptosis after thrombolysis, while the lack of these events prevented endothelial cell ferroptosis, finally resulting in BBB protection.

4. Discussion

In the present study, we observed a significant association between higher serum levels of LCN2 and ferritin and an increased risk of HT in patients with AIS after IVT. Further animal and cell experiments suggested that, LCN2 aggravated endothelial cell ferroptosis and ultimately contributed to BBB disruption and HT after thrombolysis, and the regulation of the HMGB1/Nrf2/HO-1 pathway underlies these effects. Collectively, these findings revealed a critical role of LCN2 in IVT-induced HT and provided new insights for the prevention of IVT-induced HT in clinical settings.

HT is a frequent complication of AIS after IVT, which seriously affects patient prognosis [2,3]. BBB disruption is the pathological basis of

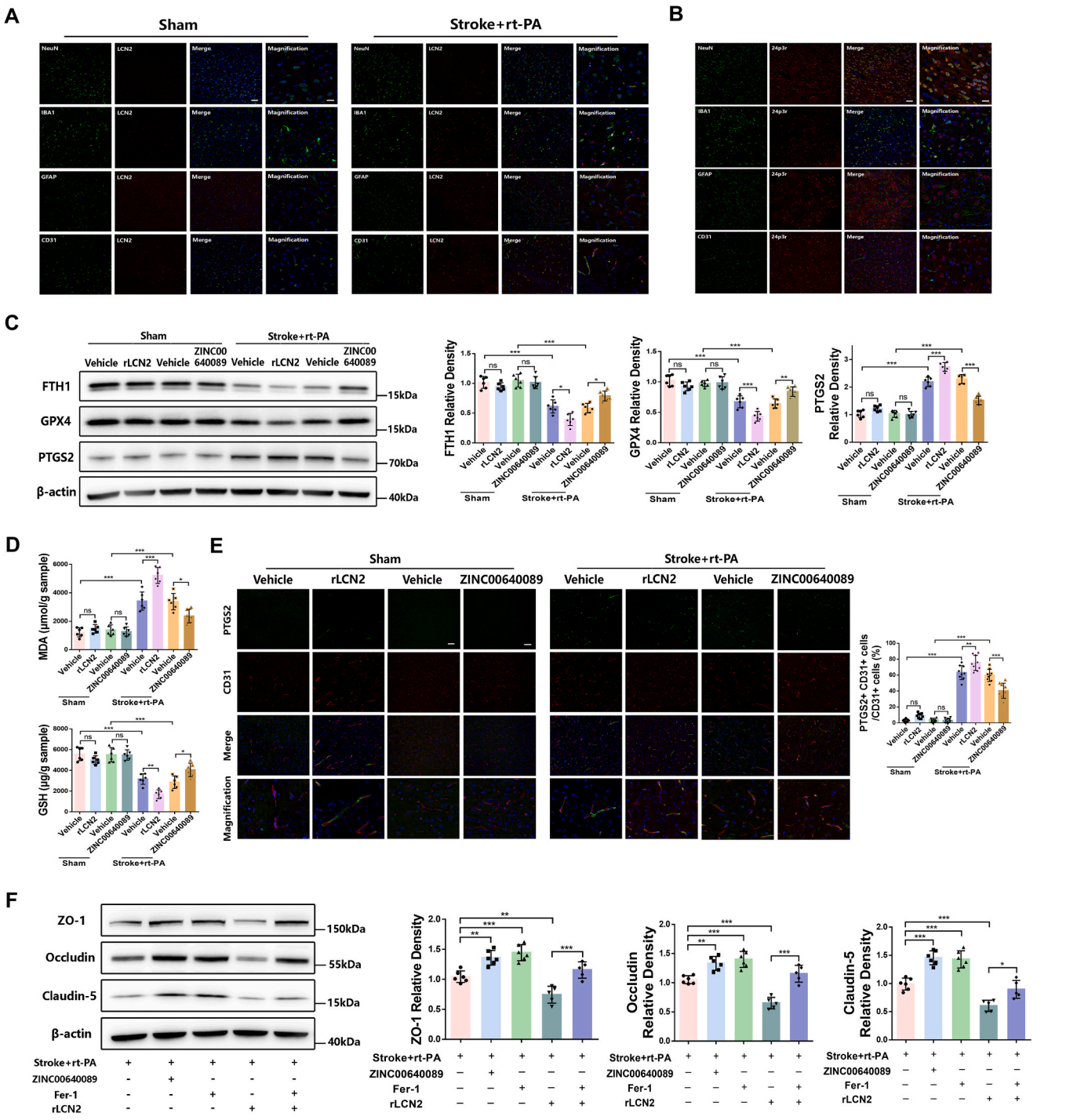

Fig. 5. LCN2 promoted endothelial cell ferroptosis to aggravate BBB disruption in the thromboembolic stroke rats after thrombolysis. (A) Representative images of NeuN, IBAl, GFAP or CD31 (green), and LCN2 (red) immunofluorescence staining in the ischemic cortex of rats 24 h after thrombolysis, with enlarged and merged image showed for co-localization. n = 3/group. Scale bar: 40 μm (merged pictures) and 20 μm (magnified pictures); (B) Representative images of NeuN, IBAl, GFAP, or CD31 (green) and 24p3r (red) immunofluorescence staining in the ischemic cortex of rats 24 h after thrombolysis, with enlarged and merged image showed for co-localization. n = 3/group. Scale bar: 40 μm (merged pictures) and 20 μm (magnified pictures); (C) Expressions of FTH1, GPX4, and PTGS2 in the ipsilateral hemisphere of rats 24 h after thrombolysis. n = 6/group. $^{*}p < 0.05$, $^{**}p < 0.01$, $^{***}p < 0.001$ by one-way ANOVA ($F = 40.02$, $p < 0.001$ for WB analysis of FTH1; $F = 38.39$, $p < 0.001$ for WB analysis of GPX4 and $F = 146.51$, $p < 0.001$ for WB analysis of PTGS2 respectively); (D) The content of MDA (μmol/g tissue) and GSH (μg/g tissue) in the ipsilateral hemisphere of rats 24 h after thrombolysis. n = 6/group. $^{*}p < 0.05$, $^{**}p < 0.01$, $^{***}p < 0.001$ by one-way ANOVA ($F = 57.79$, $p < 0.001$ for analysis of MDA content and $F = 40.5$, $p < 0.001$ for analysis of GSH content); (E) Representative immunofluorescence images of CD31 (red) and PTGS2 (green) signals and their enlarged and merged images in the ischemic cortex of rats 24 h after thrombolysis. The percentages of $PTGS2^{+}$ $CD31^{+}$ cells in the total number of $CD31^{+}$ cells were also showed. n = 3/group. Scale bar: 40 μm (merged pictures) and 20 μm (magnified pictures). $^{*}p < 0.05$, $^{**}p < 0.01$, $^{***}p < 0.001$ by one-way ANOVA ($F = 204.54$, $p < 0.001$); (F) Expressions of ZO-1, occludin, and claudin-5 in the ipsilateral hemisphere of rats 24 h after thrombolysis. n = 5–6/group. $^{*}p < 0.05$, $^{**}p < 0.01$, $^{***}p < 0.001$ by one-way ANOVA ($F = 26.68$, $p < 0.001$ for WB analysis of ZO-1; $F = 34.98$, $p < 0.001$ for WB analysis of occludin; and $F = 46.97$, $p < 0.001$ for WB analysis of claudin-5 respectively). (For interpretation of the references to color in this figure legend, the reader is referred to the Web version of this article.)

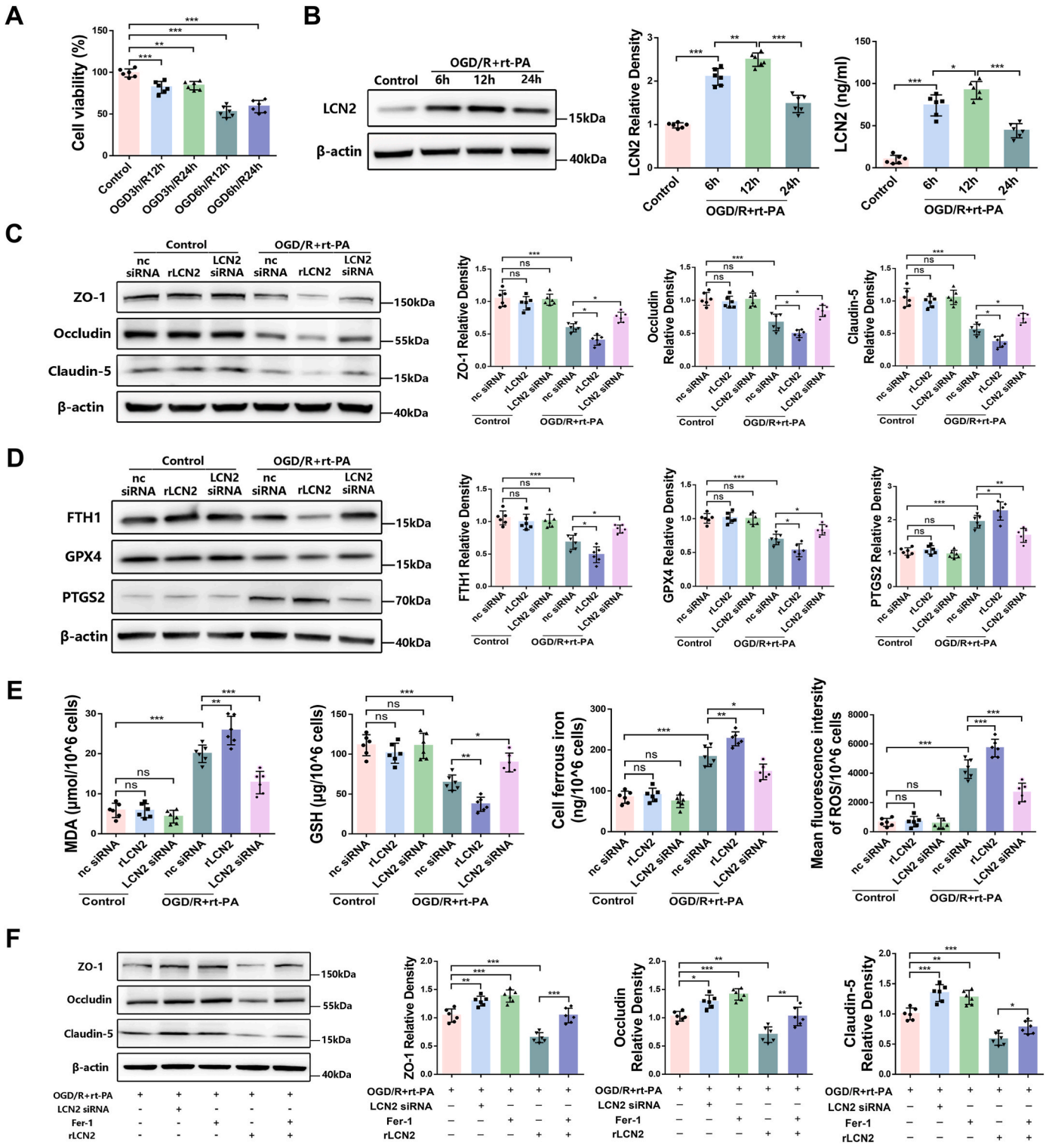

Fig. 6. LCN2 aggravated ferroptosis to promote TJPs loss in Bend.3 endothelial cells after OGD/R + rt-PA stimulus. (A) Bend.3 cell viability under different OGD/R conditions according to CCK8 assay. n = 6/group. $^{**}p < 0.01$, $^{***}p < 0.001$ by one-way ANOVA (F = 55.77, $p < 0.001$); (B) Expressions of LCN2 in Bend.3 cells at different time points after re-oxygenation according to WB and ELISA analysis. n = 6/group. $^{*}p < 0.05$, $^{**}p < 0.01$, $^{***}p < 0.001$ by one-way ANOVA (F = 101.88, $p < 0.001$ for WB analysis of LCN2 and F = 85.64, $p < 0.001$ for ELISA analysis of LCN2); (C) Expressions of ZO-1, occludin, and claudin-5 in Bend.3 cells 12 h after re-oxygenation. n = 6/group. $^{*}p < 0.05$, $^{***}p < 0.001$ by one-way ANOVA (F = 49.73, $p < 0.001$ for WB analysis of ZO-1; F = 30.73, $p < 0.001$ for WB analysis of occludin and F = 50.87, $p < 0.001$ for WB analysis of claudin-5 respectively); (D) Expressions of FTH1, GPX4 and PTGS2 in Bend.3 cells 12 h after re-oxygenation. n = 6/group. $^{*}p < 0.05$, $^{**}p < 0.01$, $^{***}p < 0.001$ by one-way ANOVA (F = 27.12, $p < 0.001$ for WB analysis of FTH1; F = 36.14, $p < 0.001$ for WB analysis of GPX4 and F = 52.22, $p < 0.001$ for WB analysis of PTGS2 respectively); (E) The contents of MDA, GSH, cell iron, and ROS in Bend.3 cells 12 h after re-oxygenation. n = 6/group. $^{*}p < 0.05$, $^{**}p < 0.01$, $^{***}p < 0.001$ by one-way ANOVA (F = 82.09, $p < 0.001$ for analysis of MDA content; F = 34.59, $p < 0.001$ for analysis of GSH content; F = 71.33, $p < 0.001$ for analysis of cell iron content and F = 115.55, $p < 0.001$ for analysis of ROS content respectively); (F) Expressions of ZO-1, occludin, and claudin-5 in Bend.3 cells 12 h after re-oxygenation. n = 6/group. $^{*}p < 0.05$, $^{**}p < 0.01$, $^{***}p < 0.001$ by one-way ANOVA (F = 42.71, $p < 0.001$ for WB analysis of ZO-1; F = 29.45, $p < 0.001$ for WB analysis of occludin and F = 49.39, $p < 0.001$ for WB analysis of claudin-5 respectively).

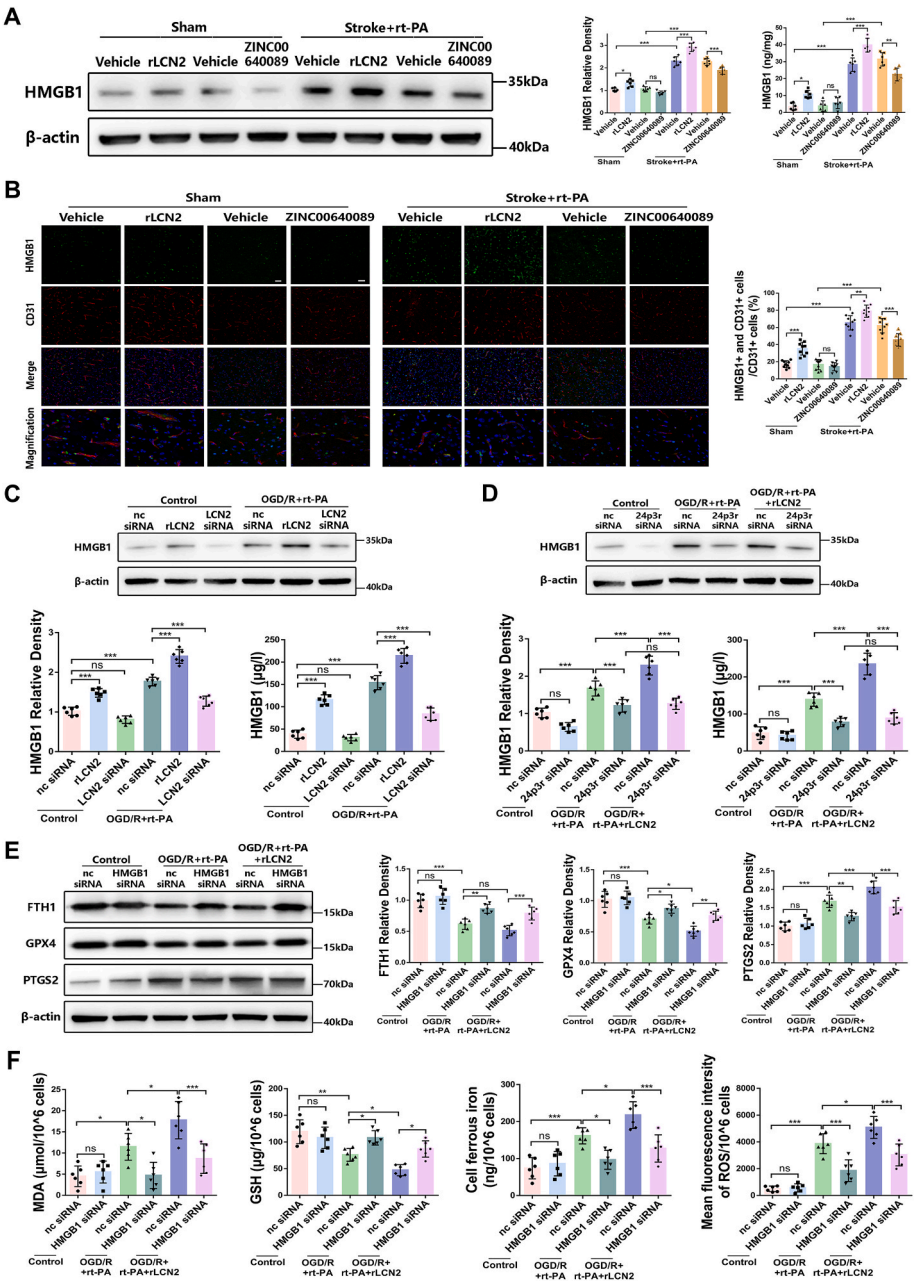

Fig. 7. HMGB1 is involved in LCN2-mediated endothelial cell ferroptosis. (A) Expression of HMGB1 in the ipsilateral hemisphere of rats 24 h after thrombolysis according to WB and ELISA analysis. n = 6/group. $^{*}p < 0.05$, $^{**}p < 0.01$, $^{***}p < 0.001$ by one-way ANOVA ($F = 151.88$, $p < 0.001$ for WB analysis of HMGB1 and $F = 103.77$, $p < 0.001$ for ELISA analysis of HMGB1); (B) Representative images of HMGB1 (green) and CD31 (red) immunofluorescence staining and their enlarged and merged images in the ischemic cortex of rats 24 h after thrombolysis. The percentages of $HMGB1^{+}$ $CD31^{+}$ cells in the total number of $CD31^{+}$ cells were showed. n = 3/group. Scale bar: 40 μm (merged pictures) and 20 μm (magnified pictures). $^{**}p < 0.01$, $^{***}p < 0.001$ by one-way ANOVA ($F = 120.65$, $p < 0.001$); (C) Expression of HMGB1 in Bend.3 cells 12 h after re-oxygenation according to WB and ELISA analysis. n = 6/group. $^{***}p < 0.001$ by one-way ANOVA ($F = 133.82$, $p < 0.001$ for WB analysis of HMGB1 and $F = 182.56$, $p < 0.001$ for ELISA analysis of HMGB1); (D) Expression of HMGB1 in Bend.3 cells 12 h after re-oxygenation according to WB and ELISA analysis. n = 6/group. $^{***}p < 0.001$ by one-way ANOVA ($F = 62.69$, $p < 0.001$ for WB analysis of HMGB1 and $F = 96.11$, $p < 0.001$ for ELISA analysis of HMGB1); (E). Expressions of FTH1, GPX4 and PTGS2 in Bend.3 cells 12 h after re-oxygenation. n = 6/group. $^{*}p < 0.05$, $^{**}p < 0.01$, $^{***}p < 0.001$ by one-way ANOVA ($F = 27.74$, $p < 0.001$ for WB analysis of FTH1; $F = 28.78$, $p < 0.001$ for WB analysis of GPX4 and $F = 41.96$, $p < 0.001$ for WB analysis of PTGS2 respectively); (F) The contents of MDA, GSH, cell iron and ROS in Bend.3 cells 12 h after re-oxygenation. n = 6/group. $^{*}p < 0.05$, $^{**}p < 0.01$, $^{***}p < 0.001$ by one-way ANOVA ($F = 15.04$, $p < 0.001$ for analysis of MDA content; $F = 16.33$, $p < 0.001$ for analysis of GSH content; $F = 18.63$, $p < 0.001$ for analysis of cell iron and $F = 45.49$, $p < 0.001$ for analysis of ROS content respectively). (For interpretation of the references to color in this figure legend, the reader is referred to the Web version of this article.)

HT [4–7]. In this study, we demonstrated that higher baseline serum ferritin and LCN2 levels were independently correlated with an increased risk of HT in patients with AIS following IVT based on the cytokine chip results. According to previous literature, under normal circumstances, the production of LCN2 in the brain is low, whereas upon injury, infection, or other inflammatory stimuli, it is rapidly upregulated, secreted outside the cells, and enters the cell to exert different effects through endocytosis by binding to its specific cell surface receptor, 24p3r [51,52]. Currently, in patients with AIS, studies have found that high circulating LCN2 levels were associated with an

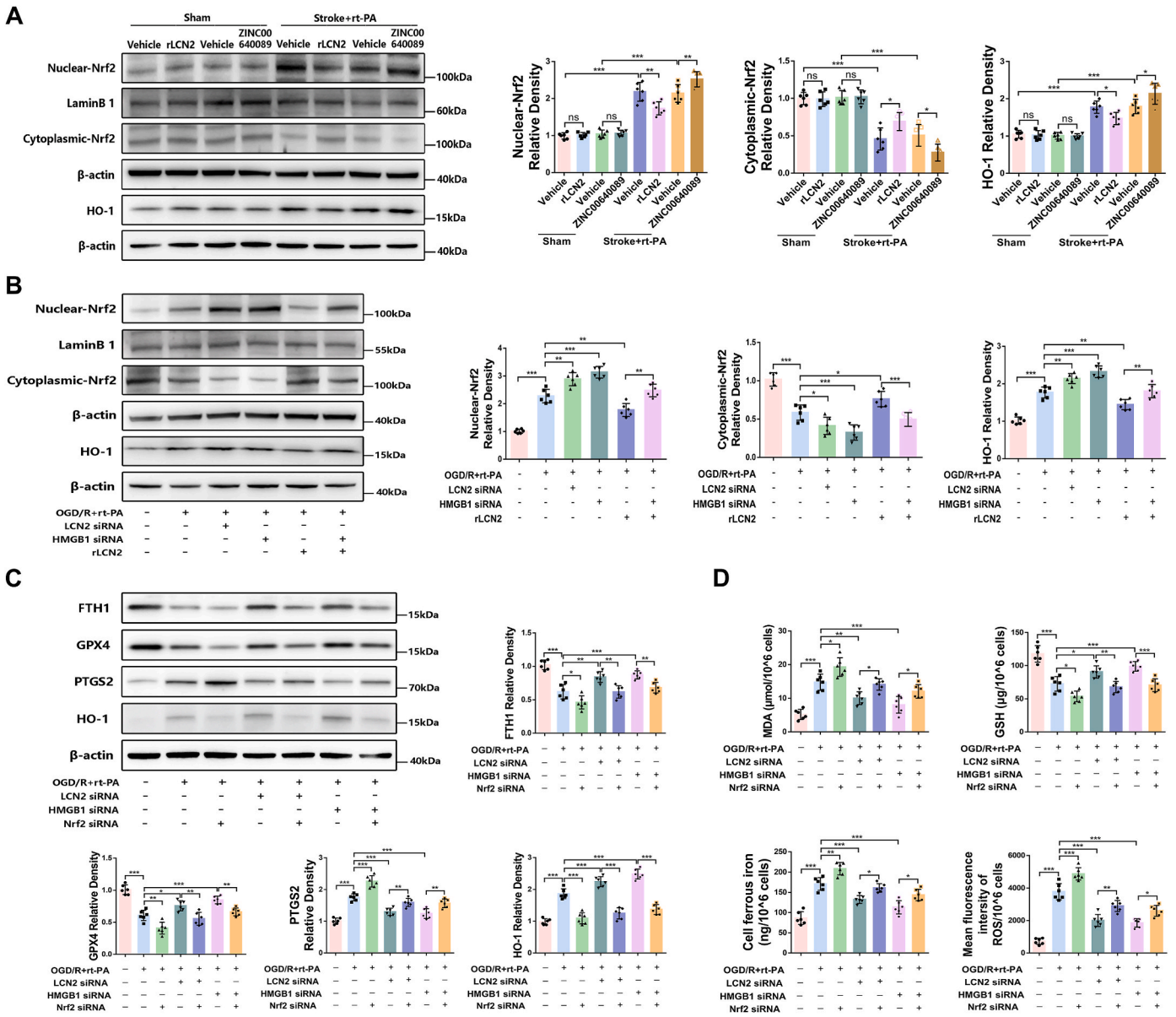

Fig. 8. Nrf2/HO-1 signaling is involved in LCN2/HMGB1-mediated endothelial cell ferroptosis. (A) Nuclear- and cytoplasmic-Nrf2 and HO-1 protein levels in the ipsilateral hemisphere of rats 24 h after thrombolysis. n = 6/group. $^{*}p < 0.05$, $^{**}p < 0.01$, $^{***}p < 0.001$ by one-way ANOVA ($F = 85.2$, $p < 0.001$ for WB analysis of nuclear-Nrf2; $F = 29.44$, $p < 0.001$ for WB analysis of cytoplasmic-Nrf2 and $F = 46.9$, $p < 0.001$ for WB analysis of HO-1 respectively); (B) Nuclear- and cytoplasmic-Nrf2 and HO-1 protein levels in Bend.3 cells 12 h after re-oxygenation. n = 6/group. $^{*}p < 0.05$, $^{**}p < 0.01$, $^{***}p < 0.001$ by one-way ANOVA ($F = 79.98$, $p < 0.001$ for WB analysis of nuclear-Nrf2; $F = 40.11$, $p < 0.001$ for WB analysis of cytoplasmic-Nrf2 and $F = 65.06$, $p < 0.001$ for WB analysis of HO-1 respectively); (C) Expressions of FTH1, GPX4, PTGS2 and HO-1 in Bend.3 cells 12 h after re-oxygenation. n = 6/group. $^{*}p < 0.05$, $^{**}p < 0.01$, $^{***}p < 0.001$ by one-way ANOVA ($F = 29.82$, $p < 0.001$ for WB analysis of FTH1; $F = 37.2$, $p < 0.001$ for WB analysis of GPX4; $F = 55.98$, $p < 0.001$ for WB analysis of PTGS2 and $F = 85.62$, $p < 0.001$ for WB analysis of HO-1 respectively); (D) The contents of MDA, GSH, cell iron and ROS in Bend.3 cells 12 h after re-oxygenation. n = 6/group. $^{*}p < 0.05$, $^{**}p < 0.01$, $^{***}p < 0.001$ by one-way ANOVA ($F = 31.02$, $p < 0.001$ for analysis of MDA content; $F = 28.32$, $p < 0.001$ for analysis of GSH content; $F = 47.46$, $p < 0.001$ for analysis of cell iron and $F = 89.53$, $p < 0.001$ for analysis of ROS content respectively).

increased risk of early clinical deterioration and adverse outcomes in patients with AIS [53]. However, this is the first study to demonstrate an association with HT after IVT.

Animal experiments were performed to confirm our clinical findings. The PTS model is a newly developed stroke model that generates infarctions through the destruction of the cortical vascular endothelial cells on the top surface of the brain via laser irradiation. Our previous researches showed that, when combined with NIR-II fluorescence imaging and IR-808 dye injection, this model allows direct observation of the brain vascular network and BBB leakage in living animals. Based on this strategy, we discovered that rLCN2 administration remarkably increased BBB permeability in rats underwent PTS surgery, especially within 24 h after surgery. The thromboembolic stroke model has been identified as the most suitable animal model for the preclinical investigation of IVT therapy [54,55], as it mimics thrombosis in vivo through electrical stimulation of the carotid artery [25], followed by dissolution of the thrombus and reperfusion achieved by injecting rt-PA into the tail vein. Therefore, we used this model to investigate the effects of LCN2 on BBB disruption and HT after thrombolysis. Our results showed that, compared with sham rats, LCN2 was significantly upregulated in thromboembolic stroke rats within 24 h after thrombolysis. Additionally, rLCN2 administration further increased infarction and hemorrhage

volumes, aggravated BBB damage, and tended to exacerbate neurobehavioral deficits in these rats. Subsequent in vitro studies on Bend.3 endothelial cells supported the in vivo findings, which revealed that rLCN2 administration promoted the downregulation of TJPs induced by OGD/R + rt-PA stimulus, whereas exposure to LCN2 siRNA reversed these changes. All these results suggested a potential therapeutic approach to prevent HT after thrombolysis by inhibiting LCN2.

Next, we explored the possible mechanisms through which LCN2 affects BBB function after thrombolysis. According to our clinical results, a significant positive correlation between serum LCN2 and ferritin levels was identified in patients with HT. Ferritin is well-known as an important reservoir for excess iron [56]. After an acute ischemic stimulus, free iron and ferritin enter the brain parenchyma through the damaged BBB to promote iron overload and ROS overproduction [38], which are characteristic processes that lead to ferroptosis. Based on this, we speculated that increased LCN2 levels may be positively correlated with ferroptosis in IVT-induced HT. Notably, LCN2 is implicated in the mediation of cellular iron transport and ferroptosis. In brain microvascular endothelial cells, Mondal et al. demonstrated that administration of LCN2 significantly elevated the levels of iron and ROS, whereas LCN2 knockdown prevented the iron-mediated decrease in cell viability and inhibited the expression of ferroptosis markers [57]. In addition, in intracerebral hemorrhage (ICH) mice, the upregulation of LCN2 promoted ferroptosis by binding to SLC3A2 to regulate GSH synthesis and GPX4 expression [58]. Therefore, we hypothesized that the increased LCN2 may contribute to ferroptosis, and thereby promote BBB disruption and HT after thrombolysis [43,59]. Since cerebrovascular endothelial cells are critical components of the BBB, we investigated the effect of LCN2 on endothelial cell ferroptosis. The animal experiments revealed that rLCN2 administration markedly aggravated ferroptosis damage and increased the percentage of PTGS2-positive endothelial cells in the ischemic cortex of thromboembolic stroke rats 24 h after thrombolysis, whereas ZINC00640089 exerted opposite effects. Meanwhile, ferroptosis inhibition by fer-1 abolished the effects of rLCN2 on BBB function. In vitro studies on Bend.3 cells further demonstrated these findings. Accordingly, we suggested that the increase of LCN2 levels could mediate BBB disruption after thrombolysis by promoting the ferroptosis of endothelial cells.

HMGB1, a damage-associated molecular pattern protein [45,60], has been identified as a classic regulatory protein of ferroptosis released by ferroptosis cells in an autophagy-dependent manner. In recent years, several studies have reported a great influence of LCN2 on HMGB1 by binding to its cell surface receptor, 24p3r [61–63]. For example, in the heart tissue, one study showed that HMGB1 was highly upregulated with an increase in LCN2 [61]. In mice with non-alcoholic steatohepatitis, high circulatory LCN2 levels induced the release of HMGB1 in the brain by binding to 24p3r, which aggravated oxidative damage and neuroinflammation [57]. In primary brain endothelial cells, increased LCN2 levels caused loss of BBB integrity, accompanied by the induction of HMGB1 [57]. Therefore, to elucidate the potential mechanism underlying LCN2-mediated ferroptosis of endothelial cells after thrombolysis, we examined the expressions of HMGB1 both in vivo and in vitro studies. Notably, our results showed significant upregulation of HMGB1 levels in the brains of thromboembolic stroke rats 24 h after thrombolysis, along with an increased percentage of HMGB1-positive endothelial cells. rLCN2 further promoted these changes, whereas ZINC00640089 prevented these events. Additionally, in Bend.3 cells, transfection with HMGB1 siRNA alleviated ferroptosis damage induced by rLCN2 in Bend.3 cells upon OGD/R + rt-PA stimulus, thus suggesting that HMGB1 is critically involved in LCN2-mediated ferroptosis of endothelial cells after thrombolysis.

The Nrf2/HO-1 axis is an important classical pathway involved in the regulation of oxidative stress and ferroptosis [47,48]. After AIS, Nrf2 dissociates from Keap1 and enters the nucleus for activation, which upregulates HO-1 and represses oxidative stress and ferroptosis [64,65]. Several recent studies have reported that HMGB1 promotes ferroptosis by regulating the Nrf2/HO-1 pathway. In ICH mice, studies have showed that inhibition of HMGB1 promoted nuclear accumulation of Nrf2 in the area around the hematoma, accompanied by the remission of oxidative stress, brain iron accumulation, and cell death [66]. In high glucose-induced mesangial cells, HMGB1 knockdown suppressed the production of ROS and the expression of ferroptosis-related proteins by upregulating Nrf2-mediated antioxidant genes [50]. Based on these, we clarified the involvement of Nrf2/HO-1 pathway in LCN2/HMGB1-mediated endothelial cell ferroptosis after thrombolysis. In both in vivo and in vitro studies, we discovered that the nuclear-Nrf2 and HO-1 protein levels decreased following rLCN2 administration, but increased following LCN2 and HMGB1 inhibition. In Bend.3 cells, additional transfection of HMGB1 siRNA abolished the downregulation of nuclear-Nrf2 caused by rLCN2. And transfection of Nrf2 siRNA inhibited the expression of HO-1 and reversed the ferroptosis inhibition caused by LCN2 siRNA and HMGB1 siRNA. Therefore, it is feasible to demonstrate that Nrf2/HO-1 pathway inhibition plays a critical role in LCN2/HMGB1-mediated endothelial cell ferroptosis after thrombolysis.

Although we demonstrated the critical role of LCN2 in BBB disruption and HT after thrombolysis as well as its potential mechanism in this study, some limitations still exist. First, several lines of evidence indicate that LCN2 can be secreted by different cells in the brain or recruited from circulation after AIS. The released LCN2 then acts on a variety of cell types and participates in the regulation of a series of pathophysiological processes such as neuroinflammation, oxidative stress, ferroptosis, and neuronal cell death [52]. Therefore, the identification of other intracellular mechanisms which may play a relevant role in LCN2-mediated BBB disruption after thrombolysis deserves further investigation. In addition, according to our study, baseline serum LCN2 levels are independently associated with HT in patients with AIS after IVT, and the increase in LCN2 disrupts BBB integrity, mainly in the acute phase of AIS. Therefore, we speculate that early intervention with LCN2 expression, even prior to AIS, may be protective against HT. The effects of delayed or preventive LCN2 inhibition should be tested and compared in future studies.

5. Conclusion

In this study, we found that higher serum ferritin and LCN2 levels were independently associated with an increased risk of HT after IVT in patients with AIS. Further, preclinical studies suggested that increased LCN2 aggravated BBB disruption and HT after thrombolysis by promoting ferroptosis of endothelial cells through the HMGB1/Nrf2/HO-1 pathway, whereas the inhibition of these events exerted opposite effects. To the best of our knowledge, this is the first study to report the critical role of LCN2 in BBB disruption and HT following IVT, and targeting LCN2 may provide new mechanistic insights in the search for interventions to prevent HT.

Fundings

This work was supported by the National Natural Science Foundation of China (82271303), and the Talent Reserve Program of the First Hospital of Jilin University (JDYYCB-2023002) to ZNG; the Norman Bethune Health Science Center of Jilin University (2022JBGS03), Science and Technology Department of Jilin Province (YDZJ202302CXJD061, 20220303002SF) and Jilin Provincial Key Laboratory (YDZJ202302CXJD017) to YY.

Data availability

The raw data for this study are available from the corresponding author upon request.

CRediT authorship contribution statement

Jie Liu: Writing – original draft, Investigation, Data curation. **Shu-Yan Pang:** Methodology, Investigation. **Sheng-Yu Zhou:** Software, Methodology. **Qian-Yan He:** Writing – review & editing, Methodology. **Ruo-Yu Zhao:** Writing – review & editing. **Yang Qu:** Writing – review & editing. **Yi Yang:** Funding acquisition. **Zhen-Ni Guo:** Writing – review & editing, Funding acquisition.

Declaration of competing interest

None.

Data availability

Data will be made available on request.

Acknowledgements

The authors thank all the staff members from the First Hospital of Jilin University for their contributions to this study. We would like to thank Editage (www.editage.cn) for English language editing.

Appendix A. Supplementary data

Supplementary data to this article can be found online at https://doi.org/10.1016/j.redox.2024.103342.

References

[1] W.J. Powers, A.A. Rabinstein, T. Ackerson, O.M. Adeoye, N.C. Bambakidis, K. Becker, J. Biller, M. Brown, B.M. Demaerschalk, B. Hoh, E.C. Jauch, C. S. Kidwell, T.M. Leslie-Mazwi, B. Ovbiagele, P.A. Scott, K.N. Sheth, A. M. Southerland, D.V. Summers, D.L. Tirschwell, Guidelines for the early management of patients with acute ischemic stroke: 2019 update to the 2018 guidelines for the early management of acute ischemic stroke: a guideline for healthcare professionals from the American heart association/American stroke association, Stroke 50 (2019) e344–e418.

[2] H. Kunte, M.A. Busch, K. Trostdorf, B. Vollnberg, L. Harms, R.I. Mehta, R. J. Castellani, P. Mandava, T.A. Kent, J.M. Simard, Hemorrhagic transformation of ischemic stroke in diabetics on sulfonylureas, Ann. Neurol. 72 (2012) 799–806.

[3] K. Shi, M. Zou, D.M. Jia, S. Shi, X. Yang, Q. Liu, J.F. Dong, K.N. Sheth, X. Wang, F. D. Shi, tPA mobilizes immune cells that exacerbate hemorrhagic transformation in stroke, Circ. Res. 128 (2021) 62–75.

[4] H. Chen, B. Guan, X. Chen, X. Chen, C. Li, J. Qiu, D. Yang, K.J. Liu, S. Qi, J. Shen, Baicalin attenuates blood-brain barrier disruption and hemorrhagic transformation and improves neurological outcome in ischemic stroke rats with delayed t-PA treatment: involvement of ONOO(-)-MMP-9 pathway, Transl Stroke Res 9 (2018) 515–529.

[5] O. Ozkul-Wermester, E. Guegan-Massardier, A. Triquenot, A. Borden, G. Perot, E. Gérardin, Increased blood-brain barrier permeability on perfusion computed tomography predicts hemorrhagic transformation in acute ischemic stroke, Eur. Neurol. 72 (2014) 45–53.

[6] J. Hom, J.W. Dankbaar, B.P. Soares, T. Schneider, S.C. Cheng, J. Bredno, B.C. Lau, W. Smith, W.P. Dillon, M. Wintermark, Blood-brain barrier permeability assessed by perfusion CT predicts symptomatic hemorrhagic transformation and malignant edema in acute ischemic stroke, AJNR Am J Neuroradiol 32 (2011) 41–48.

[7] A. Hoffmann, J. Bredno, M.F. Wendland, N. Derugin, J. Hom, T. Schuster, C. Zimmer, H. Su, P.T. Ohara, W.L. Young, M. Wintermark, MRI blood-brain barrier permeability measurements to predict hemorrhagic transformation in a rat model of ischemic stroke, Transl Stroke Res 3 (2012) 508–516.

[8] D.W. Dekens, U.L.M. Eisel, L. Gouweleeuw, R.G. Schoemaker, P.P. De Deyn, P.J. W. Naudé, Lipocalin 2 as a link between ageing, risk factor conditions and age-related brain diseases, Ageing Res. Rev. 70 (2021) 101414.

[9] F. Bi, C. Huang, J. Tong, G. Qiu, B. Huang, Q. Wu, F. Li, Z. Xu, R. Bowser, X.G. Xia, H. Zhou, Reactive astrocytes secrete lcn2 to promote neuron death, Proc. Natl. Acad. Sci. U. S. A. 110 (2013) 4069–4074.

[10] K. Suk, Lipocalin-2 as a therapeutic target for brain injury: an astrocentric perspective, Prog. Neurobiol. 144 (2016) 158–172.

[11] A.C. Ferreira, D.M. S, J.C. Sousa, M. Correia-Neves, N. Sousa, J.A. Palha, F. Marques, From the periphery to the brain: lipocalin-2, a friend or foe? Prog. Neurobiol. 131 (2015) 120–136.

[12] S. Chen, X.C. Chen, X.H. Lou, S.Q. Qian, Z.W. Ruan, Determination of serum neutrophil gelatinase-associated lipocalin as a prognostic biomarker of acute spontaneous intracerebral hemorrhage, Clin. Chim. Acta 492 (2019) 72–77.

[13] A. Huțanu, M. Iancu, R. Bălașa, S. Maier, M. Dobreanu, Predicting functional outcome of ischemic stroke patients in Romania based on plasma CRP, sTNFR-1, D-Dimers, NGAL and NSE measured using a biochip array, Acta Pharmacol. Sin. 39 (2018) 1228–1236.

[14] W.A. Keshk, D.H. Zineldeen, Y.A. El-Heneedy, A.A. Ghali, Thrombomodulin, alarmin signaling, and copeptin: cross-talk between obesity and acute ischemic stroke initiation and severity in Egyptians, Neurol. Sci. 39 (2018) 1093–1104.

[15] M. Jin, J.H. Kim, E. Jang, Y.M. Lee, H. Soo Han, D.K. Woo, D.H. Park, H. Kook, K. Suk, Lipocalin-2 deficiency attenuates neuroinflammation and brain injury after transient middle cerebral artery occlusion in mice, J. Cerebr. Blood Flow Metabol. 34 (2014) 1306–1314.

[16] G. Wang, Y.C. Weng, I.C. Chiang, Y.T. Huang, Y.C. Liao, Y.C. Chen, C.Y. Kao, Y. L. Liu, T.H. Lee, W.H. Chou, Neutralization of lipocalin-2 diminishes stroke-reperfusion injury, Int. J. Mol. Sci. 21 (2020).

[17] B. Chiou, E.H. Neal, A.B. Bowman, E.S. Lippmann, I.A. Simpson, J.R. Connor, Endothelial cells are critical regulators of iron transport in a model of the human blood-brain barrier, J. Cerebr. Blood Flow Metabol. : official journal of the International Society of Cerebral Blood Flow and Metabolism 39 (2019) 2117–2131.

[18] M. Zhang, W. Li, T. Wang, Q. Zhang, Association between baseline serum ferritin and short-term outcome of intracerebral hemorrhage: a meta-analysis, J. Stroke Cerebrovasc. Dis. : the official journal of National Stroke Association 28 (2019) 1799–1805.

[19] B. Xu, R. Yang, J. Fu, B. Yang, J. Chen, C. Tan, H. Chen, X. Wang, LncRSPH9-4 facilitates meningitic Escherichia coli-caused blood-brain barrier disruption via miR-17-5p/MMP3 Axis, Int. J. Mol. Sci. 22 (2021).

[20] H. Matsuno, S. Tsuchimine, K. O'Hashi, K. Sakai, K. Hattori, S. Hidese, S. Nakajima, S. Chiba, A. Yoshimura, N. Fukuzato, M. Kando, M. Tatsumi, S. Ogawa, N. Ichinohe, H. Kunugi, K. Sohya, Association between vascular endothelial growth factor-mediated blood-brain barrier dysfunction and stress-induced depression, Mol. Psychiatr. 27 (2022) 3822–3832.

[21] Y. Hu, Y. Bi, D. Yao, P. Wang, Y. Li, Omi/HtrA2 protease associated cell apoptosis participates in blood-brain barrier dysfunction, Front. Mol. Neurosci. 12 (2019) 48.

[22] X. Xu, D. Wang, F. Wang, C. Norton, X. Liu, M. Selim, The risk of hemorrhagic transformation after thrombolysis for acute ischemic stroke in Chinese versus north Americans: a comparative study, J. Stroke Cerebrovasc. Dis. 27 (2018) 2381–2387.

[23] R. Celis, N. Planell, J.L. Fernández-Sueiro, R. Sanmartí, J. Ramírez, I. González-Álvaro, J.L. Pablos, J.D. Cañete, Synovial cytokine expression in psoriatic arthritis and associations with lymphoid neogenesis and clinical features, Arthritis Res. Ther. 14 (2012) R93.

[24] J. Li, P. Xu, Y. Hong, Y. Xie, M. Peng, R. Sun, H. Guo, X. Zhang, W. Zhu, J. Wang, X. Liu, Lipocalin-2-mediated astrocyte pyroptosis promotes neuroinflammatory injury via NLRP3 inflammasome activation in cerebral ischemia/reperfusion injury, J. Neuroinflammation 20 (2023) 148.

[25] Y.Z. Ma, L. Li, J.K. Song, Z.R. Niu, H.F. Liu, X.S. Zhou, F.S. Xie, G.H. Du, A novel embolic middle cerebral artery occlusion model induced by thrombus formed in common carotid artery in rat, J. Neurol. Sci. 359 (2015) 275–279.

[26] Q. He, Y. Ma, C. Fang, Z. Deng, F. Wang, Y. Qu, M. Yin, R. Zhao, D. Zhang, F. Guo, Y. Yang, J. Chang, Z.N. Guo, Remote ischemic conditioning attenuates blood-brain barrier disruption after recombinant tissue plasminogen activator treatment via reducing PDGF-CC, Pharmacol. Res. 187 (2023) 106641.

[27] J. Zheng, Z. Sun, F. Liang, W. Xu, J. Lu, L. Shi, A. Shao, J. Yu, J. Zhang, AdipoRon attenuates neuroinflammation after intracerebral hemorrhage through AdipoR1-AMPK pathway, Neuroscience 412 (2019) 116–130.

[28] E.Z. Longa, P.R. Weinstein, S. Carlson, R. Cummins, Reversible middle cerebral artery occlusion without craniectomy in rats, Stroke 20 (1989) 84–91.

[29] F.A. Desland, A. Afzal, Z. Warraich, J. Mocco, Manual versus automated rodent behavioral assessment: comparing efficacy and ease of bederson and Garcia neurological deficit scores to an open field video-tracking system, J. Cent. Nerv. Syst. Dis. 6 (2014) 7–14.

[30] Y. Hua, T. Nakamura, R.F. Keep, J. Wu, T. Schallert, J.T. Hoff, G. Xi, Long-term effects of experimental intracerebral hemorrhage: the role of iron, J. Neurosurg. 104 (2006) 305–312.

[31] L. Zhang, T. Schallert, Z.G. Zhang, Q. Jiang, P. Arniego, Q. Li, M. Lu, M. Chopp, A test for detecting long-term sensorimotor dysfunction in the mouse after focal cerebral ischemia, J. Neurosci. Methods 117 (2002) 207–214.

[32] G.A. Metz, I.Q. Whishaw, Cortical and subcortical lesions impair skilled walking in the ladder rung walking test: a new task to evaluate fore- and hindlimb stepping, placing, and co-ordination, J. Neurosci. Methods 115 (2002) 169–179.

[33] R.A. Swanson, F.R. Sharp, Infarct measurement methodology, J. Cerebr. Blood Flow Metabol. : official journal of the International Society of Cerebral Blood Flow and Metabolism 14 (1994) 697–698.

[34] E. Lu, Q. Wang, S. Li, C. Chen, W. Wu, Y.X.Z. Xu, P. Zhou, W. Tu, X. Lou, G. Rao, G. Yang, S. Jiang, K. Zhou, Profilin 1 knockdown prevents ischemic brain damage by promoting M2 microglial polarization associated with the RhoA/ROCK pathway, J. Neurosci. Res. 98 (2020) 1198–1212.

[35] Z. Peng, D. Ji, L. Qiao, Y. Chen, H. Huang, Autophagy inhibition by ATG3 knockdown remits oxygen-glucose deprivation/reoxygenation-induced injury and inflammation in brain microvascular endothelial cells, Neurochem. Res. 46 (2021) 3200–3212.

[36] L. Huang, P. Sherchan, Y. Wang, C. Reis, R.L. Applegate 2nd, J. Tang, J.H. Zhang, Phosphoinositide 3-kinase gamma contributes to neuroinflammation in a rat model of surgical brain injury, J. Neurosci. 35 (2015) 10390–10401.

[37] Y. Zhang, Y. Chen, J. Wu, A. Manaenko, P. Yang, J. Tang, W. Fu, J.H. Zhang, Activation of dopamine D2 receptor suppresses neuroinflammation through αb-crystalline by inhibition of NF-κB nuclear translocation in experimental ICH mice model, Stroke 46 (2015) 2637–2646.

[38] T. Carbonell, R. Rama, Iron, oxidative stress and early neurological deterioration in ischemic stroke, Curr. Med. Chem. 14 (2007) 857–874.
[39] J. Guo, Q.Z. Tuo, P. Lei, Iron, ferroptosis, and ischemic stroke, J. Neurochem. 165 (2023) 487–520.
[40] G.S. Santiago-Sánchez, R. Noriega-Rivera, E. Hernández-O'Farrill, F. Valiyeva, B. Quiñones-Diaz, E.S. Villodre, B.G. Debeb, A. Rosado-Albacarys, P.E. Vivas-Mejía, Targeting lipocalin-2 in inflammatory breast cancer cells with small interference RNA and small molecule inhibitors, Int. J. Mol. Sci. 22 (2021).
[41] A. Bhusal, W.H. Lee, K. Suk, Lipocalin-2 in diabetic complications of the nervous system: physiology, pathology, and beyond, Front. Physiol. 12 (2021) 638112.
[42] H. Zhang, S. Zhou, M. Sun, M. Hua, Z. Liu, G. Mu, Z. Wang, Q. Xiang, Y. Cui, Ferroptosis of endothelial cells in vascular diseases, Nutrients 14 (2022).
[43] C. Liu, Q. Tian, J. Wang, P. He, S. Han, Y. Guo, C. Yang, G. Wang, H. Wei, M. Li, Blocking P2RX7 attenuates ferroptosis in endothelium and reduces HG-induced hemorrhagic transformation after MCAO by inhibiting ERK1/2 and P53 signaling pathways, Mol. Neurobiol. 60 (2023) 460–479.
[44] C. Chen, Y. Huang, P. Xia, F. Zhang, L. Li, E. Wang, Q. Guo, Z. Ye, Long noncoding RNA Meg3 mediates ferroptosis induced by oxygen and glucose deprivation combined with hyperglycemia in rat brain microvascular endothelial cells, through modulating the p53/GPX4 axis, Eur. J. Histochem. 65 (2021).
[45] Q. Wen, J. Liu, R. Kang, B. Zhou, D. Tang, The release and activity of HMGB1 in ferroptosis, Biochem. Biophys. Res. Commun. 510 (2019) 278–283.
[46] H. Chen, B. Guan, B. Wang, H. Pu, X. Bai, X. Chen, J. Liu, C. Li, J. Qiu, D. Yang, K. Liu, Q. Wang, S. Qi, J. Shen, Glycyrrhizin prevents hemorrhagic transformation and improves neurological outcome in ischemic stroke with delayed thrombolysis through targeting peroxynitrite-mediated HMGB1 signaling, Transl Stroke Res 11 (2020) 967–982.
[47] M. Dodson, R. Castro-Portuguez, D.D. Zhang, NRF2 plays a critical role in mitigating lipid peroxidation and ferroptosis, Redox Biol. 23 (2019) 101107.
[48] M. Abdalkader, R. Lampinen, K.M. Kanninen, T.M. Malm, J.R. Liddell, Targeting Nrf2 to suppress ferroptosis and mitochondrial dysfunction in neurodegeneration, Front. Neurosci. 12 (2018) 466.
[49] L. Guo, D. Zhang, X. Ren, D. Liu, SYVN1 attenuates ferroptosis and alleviates spinal cord ischemia-reperfusion injury in rats by regulating the HMGB1/NRF2/HO-1 axis, Int. Immunopharm. 123 (2023) 110802.
[50] Y. Wu, Y. Zhao, H.Z. Yang, Y.J. Wang, Y. Chen, HMGB1 regulates ferroptosis through Nrf2 pathway in mesangial cells in response to high glucose, Biosci. Rep. 41 (2021).
[51] S.S. Kang, Y. Ren, C.C. Liu, A. Kurti, K.E. Baker, G. Bu, Y. Asmann, J.D. Fryer, Lipocalin-2 protects the brain during inflammatory conditions, Mol. Psychiatr. 23 (2018) 344–350.
[52] R.Y. Zhao, P.J. Wei, X. Sun, D.H. Zhang, Q.Y. He, J. Liu, J.L. Chang, Y. Yang, Z. N. Guo, Role of lipocalin 2 in stroke, Neurobiol. Dis. 179 (2023) 106044.
[53] Y. Xie, X. Zhuo, K. Xing, Z. Huang, H. Guo, P. Gong, X. Zhang, Y. Li, Circulating lipocalin-2 as a novel biomarker for early neurological deterioration and unfavorable prognosis after acute ischemic stroke, Brain Behav 13 (2023) e2979.
[54] F. Fluri, M.K. Schuhmann, C. Kleinschnitz, Animal models of ischemic stroke and their application in clinical research, Drug Des. Dev. Ther. 9 (2015) 3445–3454.
[55] I.M. Macrae, Preclinical stroke research–advantages and disadvantages of the most common rodent models of focal ischaemia, Br. J. Pharmacol. 164 (2011) 1062–1078.
[56] D. Gill, G. Monori, I. Tzoulaki, A. Dehghan, Iron status and risk of stroke, Stroke 49 (2018) 2815–2821.
[57] A. Mondal, D. Bose, P. Saha, S. Sarkar, R. Seth, D. Kimono, M. Albadrani, M. Nagarkatti, P. Nagarkatti, S. Chatterjee, Lipocalin 2 induces neuroinflammation and blood-brain barrier dysfunction through liver-brain axis in murine model of nonalcoholic steatohepatitis, J. Neuroinflammation 17 (2020) 201.
[58] X. Liu, Y. Li, S. Chen, J. Yang, J. Jing, J. Li, X. Wu, J. Wang, J. Wang, G. Zhang, Z. Tang, H. Nie, Dihydromyricetin attenuates intracerebral hemorrhage by reversing the effect of LCN2 via the system Xc- pathway, Phytomedicine 115 (2023) 154756.
[59] Y. Abdul, W. Li, R. Ward, M. Abdelsaid, S. Hafez, G. Dong, S. Jamil, V. Wolf, M. H. Johnson, S.C. Fagan, A. Ergul, Deferoxamine treatment prevents post-stroke vasoregression and neurovascular unit remodeling leading to improved functional outcomes in type 2 male diabetic rats: role of endothelial ferroptosis, Transl Stroke Res 12 (2021) 615–630.
[60] R. Chen, R. Kang, D. Tang, The mechanism of HMGB1 secretion and release, Exp. Mol. Med. 54 (2022) 91–102.
[61] E. Song, J.W. Jahng, L.P. Chong, H.K. Sung, M. Han, C. Luo, D. Wu, S. Boo, B. Hinz, M.A. Cooper, A.A. Robertson, T. Berger, T.W. Mak, I. George, P.C. Schulze, Y. Wang, A. Xu, G. Sweeney, Lipocalin-2 induces NLRP3 inflammasome activation via HMGB1 induced TLR4 signaling in heart tissue of mice under pressure overload challenge, Am J Transl Res 9 (2017) 2723–2735.
[62] A. Asimakopoulou, A. Fülöp, E. Borkham-Kamphorst, E.V. de Leur, N. Gassler, T. Berger, B. Beine, H.E. Meyer, T.W. Mak, C. Hopf, C. Henkel, R. Weiskirchen, Altered mitochondrial and peroxisomal integrity in lipocalin-2-deficient mice with hepatic steatosis, Biochim. Biophys. Acta, Mol. Basis Dis. 1863 (2017) 2093–2110.
[63] N. Müller, M. Scheld, C. Voelz, N. Gasterich, W. Zhao, V. Behrens, R. Weiskirchen, M. Baazm, T. Clarner, C. Beyer, N. Sanadgol, A. Zendedel, Lipocalin-2 deficiency diminishes canonical NLRP3 inflammasome formation and IL-1β production in the subacute phase of spinal cord injury, Int. J. Mol. Sci. 24 (2023).
[64] M. Mazhar, G. Yang, H. Xu, Y. Liu, P. Liang, L. Yang, R. Spáčil, H. Shen, D. Zhang, W. Ren, S. Yang, Zhilong Huoxue Tongyu capsule attenuates intracerebral hemorrhage induced redox imbalance by modulation of Nrf2 signaling pathway, Front. Pharmacol. 14 (2023) 1197433.
[65] Y.Y. Sun, H.J. Zhu, R.Y. Zhao, S.Y. Zhou, M.Q. Wang, Y. Yang, Z.N. Guo, Remote ischemic conditioning attenuates oxidative stress and inflammation via the Nrf2/HO-1 pathway in MCAO mice, Redox Biol. 66 (2023) 102852.
[66] C.F. Chang, S. Cho, J. Wang, (-)-Epicatechin protects hemorrhagic brain via synergistic Nrf2 pathways, Ann Clin Transl Neurol 1 (2014) 258–271.
[67] K.H. Choi, M.S. Park, J.T. Kim, T.S. Nam, S.M. Choi, B.C. Kim, M.K. Kim, K.H. Cho, The serum ferritin level is an important predictor of hemorrhagic transformation in acute ischaemic stroke, Eur. J. Neurol. 19 (2012) 570–577.
[68] Q. Wu, C. Wei, S. Guo, J. Liu, H. Xiao, S. Wu, B. Wu, M. Liu, Acute iron overload aggravates blood-brain barrier disruption and hemorrhagic transformation after transient focal ischemia in rats with hyperglycemia, IBRO Neurosci Rep 13 (2022) 87–95.
[69] R.G. Rempe, A.M.S. Hartz, B. Bauer, Matrix metalloproteinases in the brain and blood-brain barrier: versatile breakers and makers, J. Cerebr. Blood Flow Metabol. 36 (2016) 1481–1507.
[70] A.K.W. Lai, T.C. Ng, V.K.L. Hung, K.C. Tam, C.W. Cheung, S.K. Chung, A.C.Y. Lo, Exacerbated VEGF up-regulation accompanies diabetes-aggravated hemorrhage in mice after experimental cerebral ischemia and delayed reperfusion, Neural Regen Res 17 (2022) 1566–1575.
[71] S. Michalak, A. Kalinowska-Lyszczarz, D. Wegrzyn, A. Thielemann, K. Osztynowicz, W. Kozubski, The levels of circulating proangiogenic factors in migraineurs, NeuroMolecular Med. 19 (2017) 510–517.
[72] D.A. Greenberg, K. Jin, Vascular endothelial growth factors (VEGFs) and stroke, Cell. Mol. Life Sci. 70 (2013) 1753–1761.
[73] S.D. Wang, Y.Y. Fu, X.Y. Han, Z.J. Yong, Q. Li, Z. Hu, Z.G. Liu, Hyperbaric oxygen preconditioning protects against cerebral ischemia/reperfusion injury by inhibiting mitochondrial apoptosis and energy metabolism disturbance, Neurochem. Res. 46 (2021) 866–877.